FAILURE RESISTANCE AND FAILURE MODES OF BOLTED JOINTS BETWEEN METAL AND THICK COMPOSITE PLATES

By

Brandon Zachary Bouchard

A THESIS

Submitted to Michigan State University in partial fulfillment of the requirements for a degree of

MASTER OF SCIENCE

MECHANICAL ENGINEERING

2011

ABSTRACT

FAILURE RESISTANCE AND FAILURE MODES OF BOLTED JOINTS BETWEEN METAL AND THICK COMPOSITE PLATES

By

Brandon Zachary Bouchard

Composite materials are increasing in popularity for use in various industries. Recently the size of structures produced from these materials has begun to increase. As the size and thickness of such structures increase, it is inevitable that joints will be necessary. Mechanical fastening is a popular choice in joining composites because of the ability to transfer high loads and the ease of assembly and disassembly. However, drilling operations expose the fibers to environmental factors, and the high contact stresses between the bolt and the hole lead to localized delaminations, decreasing the joint strength. In this thesis, the effects of using isotropic inserts and varying the preload of thick composites in a single lap joint are examined.

In addition to failure testing, a specialized sensor to accurately measure preload with the use of a Fiber Optic Strain Gage is proposed and created. This sensor is produced for the current experiments but can be expanded to other applications.

Testing methods are initially developed and a sample size of .5" thick is decided upon. The tests then performed are on non-reinforced joints and joints reinforced with both machined isotropic inserts and the novel design. The amount of preload is also varied for tests. All of the joints described are tested to ultimate failure to determine any trends. From these tests, it can be seen that the inserts and preload improve stiffness of thick composite joints. Preload also increases the initial failure load of the joints.

This thesis is dedicated to my parent grandfather Ralph Seleski wh	s for their support through al ho was always so proud of m	Il of the hard times. Also to my ne may he rest in peace.

ACKNOWLEDGEMENTS

So many have been able to help me through my journey at Michigan State University, I will try to include everyone but inevitably some may be left out and I apologize. First I would like to thank Dr. Gaetano Restivo for his guidance and help through the course of achieving my Masters. Dr. Soonsung Hong for allowing me to use his testing machine for my research. The Composite Vehicle Research Center for the opportunity and funding to perform my research. My fellow research assistants at the CVRC for their help and a chance to escape periodically from my testing and research. And finally I would like to thank Carl Coppola for his help over the years before his recent passing.

TABLE OF CONTENTS

LIST OF TABLES	vi
LIST OF FIGURES	vii
KEY TO SYMBOLES OR ABBREVIATIONS	ix
CHAPTER 1	
INTRODUCTION	1
CHAPTER 2	
TESTING PREPERATIONS AND INITIAL TESTING	11
Testing Setup and Fixture Design	11
Material Selection and Characterization	
Initial Destructive Testing	16
Baseline Destructive Testing Results	18
Layered Test Samples	
CHAPTER 3	
INSERT TESTING	25
Materials	25
Insert Testing Results	27
CHAPTER 4	
NOVEL PRELOAD SENSOR AND PRELOAD TESTING	31
Preload Measurement Techniques	31
Construction of the Novel Preload Sensor	
Calibration of the Preload Sensor	41
Preload Testing Parameters	44
Preload Testing Results	
CHAPTER 5	
CONCLUSIONS	47

LIST OF TABLES

Table 1: Experimentally determined material properties of G10 Garolite	
Table 2: Key values for layered specimen tests	24
Table 3: Key values from insert testing.	29
Table 4: Key values from preload testing.	46

LIST OF FIGURES

Figure 1: (a) Front view and (b) Cross sectional view of damage on a 6.48 mm thick sample.	3
Figure 2: Test setup for measuring failure with preload.	6
Figure 3: The effect of E/D on bearing strength for varied W/D.	7
Figure 4: Average failure loads with varied preload	9
Figure 5: Specimen fixture for testing thick samples	11
Figure 6: Strain gage placement and installed specimen.	13
Figure 7: Stress is plotted against strain measured by the gages.	15
Figure 8: The longitudinal strain over the trnsvers strain is plotted.	15
Figure 9: FE analysis for St. Venant Effects.	17
Figure 10: Sample dimentions and test configuration for single lap shear joint tests	18
Figure 11: Pictures of the outer facing surface after initial failure.	19
Figure 12: Pictures of the interface surface of the composite after initial failure.	19
Figure 13: Graph of force vs. displacement for initial tests.	20
Figure 14: Graph of force vs. displacement during testing with grip pressure at 200 pis	21
Figure 15: Pictures corresponding to Points A, B and D in Figure 14	22
Figure 16: Bisection of failed specimen.	23
Figure 17: Load vs. displacement for layered sample tests.	24
Figure 18: Side view of single lap joint in testing Figure.	25
Figure 19: Possible novel insert designs.	26
Figure 20: Load vs. displacement graph for baseline tests	27
Figure 21: Load vs. displacement plot for steel inserts	28
Figure 22: Load vs. displacement plot for aluminum inserts.	29

Figure 23:Cross section of failed novel insert.	30
Figure 24: Torque Control Curve	33
Figure 25: Direct Tension Indicator Washers	33
Figure 26: Elongation using TOF	35
Figure 27: CW Ultrasonic Bolt Experimental Setup	35
Figure 28: 3D ESPI Image at 26 kN preload	36
Figure 29: DIC Washer Setup.	37
Figure 30: FOSG Operation	38
Figure 31: EDM Cut Bolt	39
Figure 32: Installation jig for novel preload sensor.	40
Figure 33: Novel preload sensor.	41
Figure 34: Load cell calibration.	41
Figure 35: Bolt yield determination.	42
Figure 36: Setup for calibration of the novel preload sensor.	43
Figure 37: Calibration of the novel preload sensor	44
Figure 38: Strain vs. load for loading and unloading of the novel preload sensor	44
Figure 39: Load vs. displacement results for preload tests.	46
Figure 40: Stiffness values for inserts plotted with error bars.	50
Figure 41: Initial failure values for inserts plotted with error bars.	50
Figure 42: Ultimate failure values for inserts plotted with error bars	50
Figure 43: Stiffness values for preloads plotted with error bars	51
Figure 44: Initial failure values for preloads plotted with error bars.	51
Figure 45: Ultimate failure values for preloads plotted with error bars	51

KEY TO SYMBOLES OR ABBREVIATIONS

A - Area k – Torque Coefficient

ADIC – Automatic Digital Image L - Length

Correlation OD – Outer Diameter

D - Diameter t - Thickness

DIC – Digital Image Correlation T - Torque

E – Young's Modulus TOF – Time of Flight

EDM – Electronic Discharge Machining RSG – Resistance Strain Gage

ESPI – Electronic Speckle Pattern W - Width

Interferometry δ - Deflection

F – Force ν – Poisson's Ratio

FOSG – Fiber Optic Strain Gage σ_b - Stress

gf – Gage Factor λ - Wavelength

H - Height $\Delta \lambda$ - Change in Wavelength

CHAPTER 1 INTRODUCTION

Laminated composite materials are being used in greater frequency as they can provide weight and strength advantages. The high strength and stiffness to weight ratios mean that structures can be tailored to loads. Many aerospace applications already exist for such materials, but as larger structures and vehicles are designed, better understanding of thicker composites is necessary. In Gurvich (1995) and Wisnom (1999), increasing the thickness of the composite has been shown to decrease the strength. These studies have attributed this reduction in strength to increased voids and imperfections in the matrix, increased chance of ply misalignment, and stress gradients through the thickness.

In most structures, the composite must be joined to either another composite or a metal substructure. These joints can be achieved by adhesive bonding or mechanical fasteners. Some studies such as those done by Matou (2004) have experimentally studied adhesively joined composites. This study details an investigation of the effects of thickness on a tongue and groove adhesively bonded joint. The study concluded that there were no major effects of composite thickness on this type of joint. A recent review, Banea et al (2009), of adhesive joints has also been conducted. Adhesives normally produce semi permanent joints and are not practical in applications requiring disassembly.

Bolted joints however provide many advantages including the ability to be easily assembled, disassembled, and transfer high loads. The advantages of composites can unfortunately be reduced due to the stress concentrations produced by drilling. Because the anisotropy of composites, modeling the joints is much more difficult than doing so with an isotropic material. Increasing the thickness of the composite increases the difficulty of modeling.

In the past, Basu et al (2006) along with others in the field have attempted to develop failure models for multidirectional composites. Reviews have also been compiled by Camanho et al (1997) and Thoppul (2009) over different experimental and modeling techniques.

Hou et al (2002) studied the effects of three dimensional scaling in pinned composite joints. The composites tested were comprised of an S2 glass and phenolic matrix. These materials were then hand laid to produce a ply orientation of [(0/90)/(45/-45)]. Samples were produced in thicknesses of 1.96, 5.97, 9.40, and 20.42mm. Consistent factors in the test were the Width to Diameter ratio (W/D) and the Edge to Diameter ratio (E/D). The W/D and E/D were chosen so that the sample would fail only due to bearing failure. These values were 4 for the W/D and above 2.66 for the E/D. The quantity varied to study the scaling was the Thickness to Diameter ratio (H/D). Values chosen for the H/D were 0.4, 0.75, and 1.5. These values provide for results where the hole is large or small compared to the thickness.

To conduct the study the quasi-isotropic laminate was tested in a double lap single pin joint. The samples were sandwiched by two steel plates of the same thickness as the sample. This setup was easily produced and prevented the specimen from bending. All samples were tested in this type of fixture at a constant crosshead rate of 1.27 mm/min. These tests resulted in two types of results, either the sample failed in a brittle or ductile mode. The brittle mode had sharp losses in load at failure and the ductile having little to no loss.

Samples with an H/D of .4 and .75 failed only with the brittle mode and the 1.5 H/D samples failed in ductile mode. When increasing the size by three and five times, the samples with an H/D of .4 had a decrease in the bearing strength both times. The most interesting results from this study however were those of the samples with H/D of .75 and 1.25. The bearing

strength of these samples increased when the size was increased three times, but then decreased when the size was increased five times.

Hou et al (2003) studied the effects of varying the W/D and the E/D. The laminate samples were made with glass/epoxy prepreg tape and stacked in a [0/90] ply orientation. Three thicknesses of sample were produced. These thicknesses were 3.30, 6.48, and 12.95 mm. The hole thickness for each of the thicknesses was chosen to be as close to the thickness as possible so that the H/D would remain constant. The W/D and E/D were also maintained at constant ratios of 4. This ratio was important in ensuring that the initial failure was bearing.

All samples were tested in a double lap single pin fixture. The pin was a snug fit for the hole size and the plates making up the laps were steel with half the thickness of the composite. The laps and pin were selected to ensure that only the composite failed. All of the samples were then tested in a tensile testing machine at a constant rate of 1.27 mm/min.

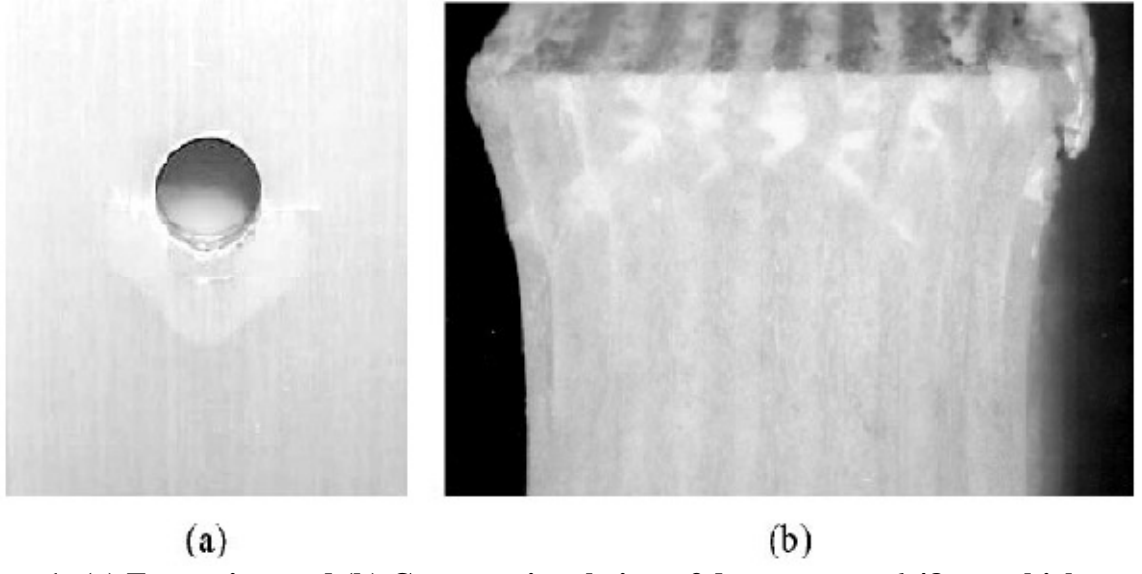


Figure 1: (a) Front view and (b) Cross sectional view of damage on a 6.48 mm thick sample.

Results showed that the two thinner types of samples failed first in bearing before ultimately failing in net tension. The bearing damage can be seen in Figure 1, where delamination and buckling can be seen as well as the start of net tension in the front view. The

12.95 mm thick samples however failed catastrophically in net tension before any signs of bearing. This was said to take place due to the higher constraint in the thickness direction. This constraint created higher resistance to buckling and delamination. These resistances therefore allowed for a buildup of stress before the catastrophic failure due to net tension.

The authors also tested the conclusion of higher constraint in the thickness causing the net tension by bolting the connection for the thinner samples. This test did prove to improve the resistance to buckling and delamination. Improving the resistances also caused the failure of the samples to be in net tension earlier then the pinned joint earlier tested.

In order to decrease the stresses around the hole, isotropic inserts have been studied in bolted composite joints. Nillsson et al (1989) performed a 2D Finite Element Analysis and experiments with adhesively bonded metal inserts in a composite bolted joint. This study was conducted with a W/D of 4 and a E/D of 2.5. The addition of these inserts resulted in a maximum reduction in the stress concentration of 55% for the steel insert. The Experimental study to verify the results was performed on a 3.6 mm thick composite. The results showed increased failure loads a maximum of 55% for the bonded and 20% for unbounded inserts.

Herrera-Franco et al (1992) also studied the use of strain relief inserts. In their experimental study, 3.55 mm thick laminates with W/D > 8 and E/D > 3 the hole diameter of 6.35 mm was tested. To view the strains, moiré fringe patterns were used. The results showed greatly reduced strains for the samples with both aluminum and steel inserts. Camanho et al (2005) has also looked into bonded metal inserts in a thin composite joint. As with the previous insert studies, reduced stress concentrations were observed. Unlike the other studies failure loads were not seen to decrease. The authors also used tapered inserts that protruded from the joint. The tapered insert was shown to increase the failure load by as much as 288%.

Other published works have looked further into the effects of preload or the amount of force initially carried by the bolt. In Khashaba et al (2006), samples composite samples produced with glass and epoxy were used to test the effects of washer size and torque. These samples were produced by the hand layup method to a thickness of 5.2 ± 0.01 mm. The loading rate for all of the experiments was kept at 2 mm/min. Before testing the torque and washer size on the joints, material tests were performed to determine compressive, tensile and shear modulus.

Keeping the preload torque to 15 Nm, the washer outer diameters were tested at 14, 18, 22, and 27mm with a constant inner diameter of 1.04. Failure load was seen to decrease with the increase in washer size. This behavior was seen as dependent upon the contact pressure and laterally constrained area of the washer. Using a constant washer OD of 18 mm, the different levels of torques tested were 0, 5, 10, and 15 Nm. With the variation of torque, increased torque was seen to increase the stiffness of the overall joint.

Pakdil et al (2007) studied the effects of different ply orientations, preload torques, and E/D and W/D ratios. The thickness of the samples was kept constant at 3 mm and the loading rate was also a constant .5 mm/min. During testing, preload was observed to change the failure mode from a net tension or shear out to a mixed failure, mainly including bearing. Bearing load as calculated by equation 1, was seen to increase by increasing the E/D ratio. Bearing load (σ_b) is the force seen by the bearing plane caused by the force on the joint (F) over the diameter (D) multiplied by the thickness (t).

$$\sigma_{b} = \frac{F}{D * t} \tag{1}$$

In Sayman (2007) the effects of composite joints with preload were studied. In the study evaluation of the failure was conducted by using a consistent thickness but varying the ply

orientation, preload and geometry of the hole. The material tested was a glass fiber/epoxy composite with an average thickness of 1.6 mm. The plies were arranged in four different orientations, [0/30], [0/45], [0/60], and [0/90]. The final samples were then produced with W/D ranging from 2-5, and E/D from 1-5. These values were picked so that the different failure modes would take place during the study.

Preloads used on the bolts were 0, 2.5, 5 Nm. Two setups were used in the determination of the failure mechanics and modes. One was a simple double lap fixture with a pin joint to evaluate the sample without preload. The other was a fixture that allowed the bolt to be loaded without the possibility of bending and minimal friction force. This second setup can be seen in Figure 2.

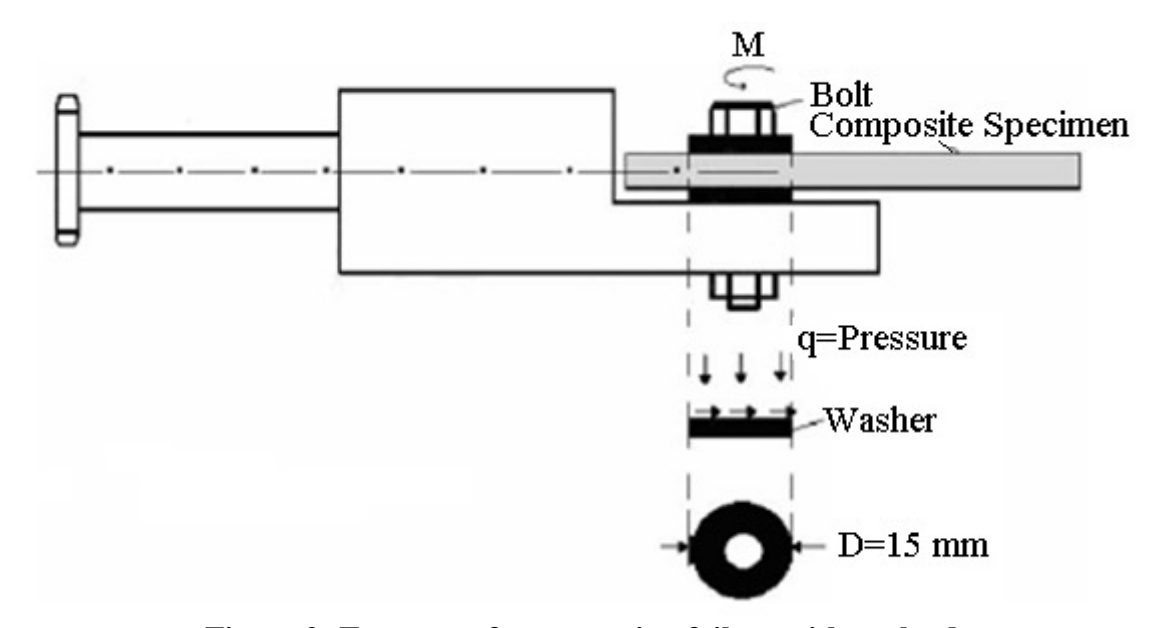


Figure 2: Test setup for measuring failure with preload.

All specimens were tested in an Instron-1114 tensile testing machine with a crosshead speed of 0.5 mm/min. The test was concluded when the bolt displacement reached 6 or 8 mm from the initial position. This finish point was selected because in bearing failure the samples

continue to carry load without catastrophic failure. Most of the samples had the first sudden loss in load at 1 to 2 mm and then continued to fail in bearing.

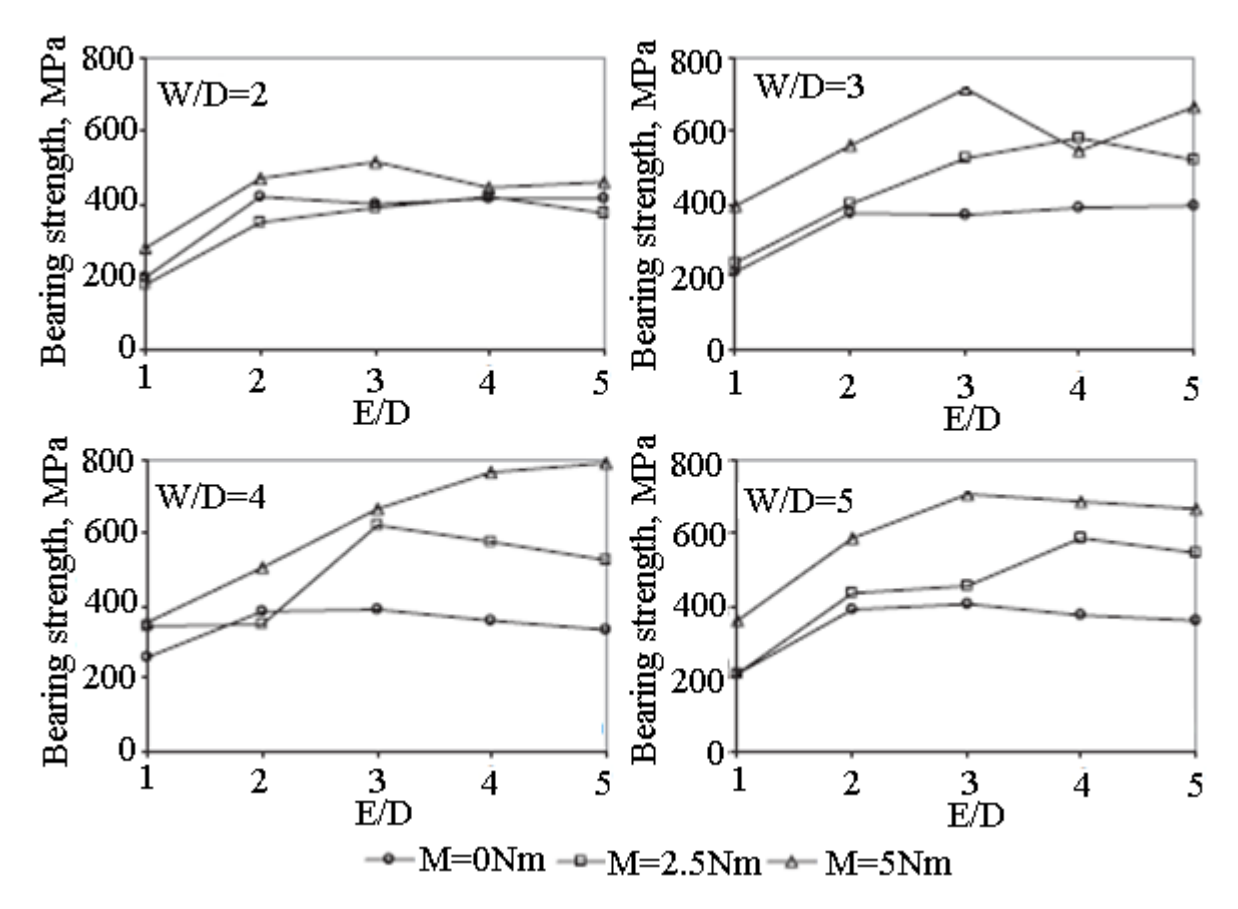


Figure 3: The effect of E/D on bearing strength for varied W/D.

Other results showed that for all configurations the [0/90] ply orientation had the highest bearing strength, while the [0/30] ply orientation had the lowest. Shown in Figure 3 increasing the E/D and W/D generally increased the bearing strength in the [0/90] samples. It can also be seen that the increased preload also increased the bearing strength.

Pekbey (2008) published a similar study, but instead of varying the ply orientation of the samples, the geometric properties of the hole and preloads were varied. The samples for this investigation were created using E-glass and epoxy resin. They were manufactured with the hand lay-up technique to a thickness of 1.6 mm and in the ply orientation of [0/90/45/-45]_s. For pin loading the standard double lap setup was used. For measuring the effects of torque the setup

was the same as used in the study by [5]. Both setups were tested in an Instron-1114 at a cross head displacement rate of .5 mm/min.

Results showed increasing the torque improved the failure strength of the samples. Other observations include that increasing both E/D and W/D increased the bearing strength of the composite panel. The highest loads were seen with the highest values for W/D, E/D, and preload. It can be noted that bearing failure was seen at W/D \geq 4 and E/D \geq 2, while values below these numbers varied between net tension and shear out.

[1] was also a similar test, but the material contained a filler and the preloads were taken to a higher level then the previous two studies. The samples were produced from a 6.35 mm thick EXTREN 500 Series flat sheet. This sheet is made of E-type glass fibers in a polyester resin and filler of clay or calcium carbonate. The fixture used to test the samples was of the double lap joint type. The samples were sandwiched between two steel plates and then mechanically fastened. The samples were tested with torques of 0, 3, and 30 Nm.

The tests were performed on an Amsler Universal testing machine. Loading took place at a rate of 10 kN/min, and displacement was measured with a transducer. The transducer measured the displacement of the bolt compared to a fixed point on the sample.

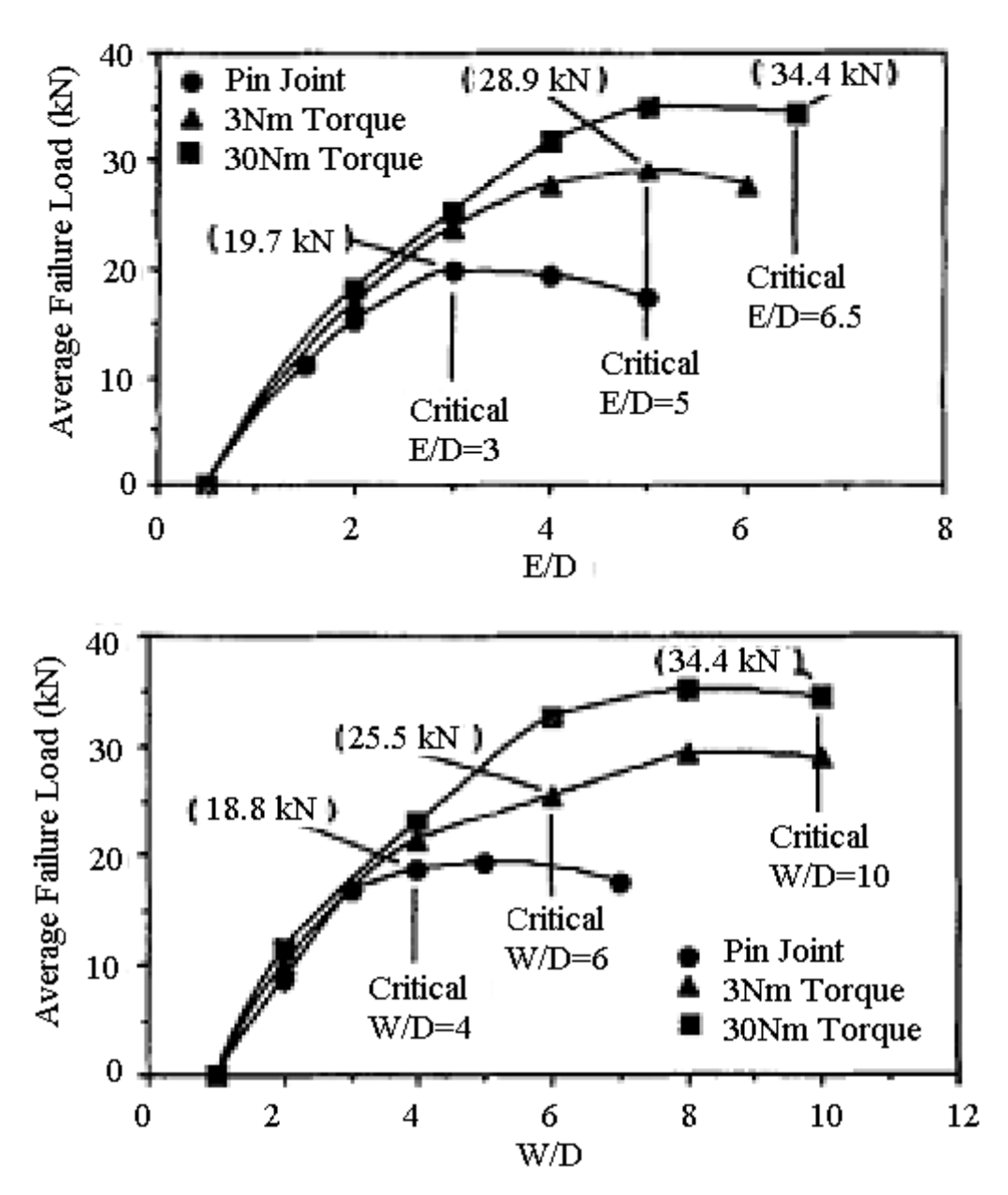


Figure 4: Average failure loads with varied preload.

As seen in Figure 4, the higher the torque on the joint the higher the failure load that the sample was able to withstand. These results also carry over to seeing higher damage loads. In relation the stiffness, the E/D does not affect it but the W/D does. Bearing failure was seen for the 3 Nm torque above a W/D of 4 and E/D of 5.

Compared to Sayman and Pekbey, an interesting difference took place with this setup.

After failure, the load is seen to rise again. This was due to the buckling of the composite

creating greater friction and pressure between the sides of the fixture. This in turn increased the resistance to buckling and delamination for a short period of time.

The author concluded with a recommendation to torque these joints at a lower value as to not assume that the structure will be correctly assembled. If one joint is improperly assembled the structure will have a significantly lower load carrying capability.

CHAPTER 2 TESTING PREPERATIONS AND INITIAL TESTING

Testing Setup and Fixture Design

All tests were performed using a MTS 810. This system can be controlled with a Flex Test Se or the MTS 793 Software. The testing machine was fitted with a 100 kN Force Transducer and a set of Series 647 Hydraulic Wedge Grips. The grips used with this machine will allow for tensile and compressive testing with maximum gripping pressure of 3000 psi (20.68 MPa) and a maximum force of 100 kN. These grips allow for a sample thickness of approximately .3" (7.62 mm). The tests performed however were on composites with a thickness of .5" (12.7 mm) and do not fit into the present setup. A specialized fixture was necessary to transfer load to the test samples.

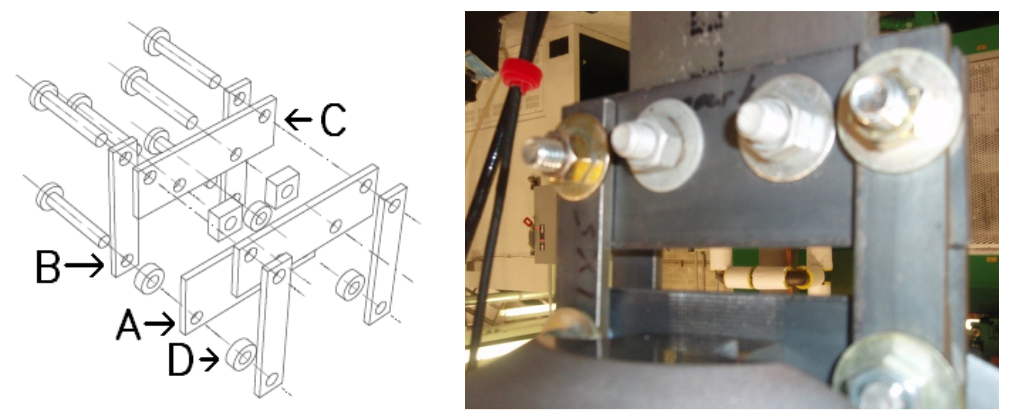


Figure 5: Specimen fixture for testing thick samples. For interpretation of the references to color in this and all other figures, the reader is referred to the electronic version of this thesis.

A design was produced that was able to fit the thick samples, allow for alignment, and fit various widths of samples. All parts of this design were produced from steel with a thickness of .25" (6.35 mm). The material selection was based on readily available materials and its ability to transfer the loads up to failure of the sample. In Figure 5, Part A is the mounting base that is gripped into the MTS. Load is then transferred through bolts to Parts B which connects the base

to the specimen fixture. The specimen clamp, Part C, finally transfers the load to the specimen. Load can be transferred from the specimen holder by either clamping the sample in with the torque of the bolts and friction, or by directly bolting the specimen to the plates.

This design provides for a number of advantages in testing. One advantage is that this fixture allows for slight realignment of the specimen when properly installed and loaded. When the apparatus is positioned into the MTS, load will equalize between the four posts and align the force through the sample. The bolts also allow for fast and easy assembly and disassembly. This ability for fast changes allows for different specimen clamps to be installed based on the size of the sample being tested. In addition to changing the specimen clamps altering the spacers, Parts D, allows for offsets to the specimen clamp. These offsets allow for the testing of single lap shear joints or other tests that require such an offset without affecting the sample or hydraulic grips.

Material Selection and Characterization

For destructive testing, a large quantity of samples must be tested in order to provide statistically significant results. The production of these samples must also remain consistent to provide less variation between tests. Because the manufacture of composites is time consuming and inconsistent when laid by hand, the decision was made to purchase the panels from a composites manufacturer. Purchasing panels allowed for faster availability, better consistency in the ply orientations and less defects then if produced individually. Several manufacturers were contacted and McMaster Carr was selected as they were able to produce the panel in the least amount of time. The initially purchased panel was a .5" (12.7 mm) thick composite panels with a [0/90] layup. This panel was constructed of Grade G-10 Garolite to Military standard MIL-I-24768.

The properties of this material were not provided by the manufacturer so experimental determination was necessary. The properties will later be used to produce finite element models for comparison with elastic range testing. To find the properties, an 8" (203 mm) long sample with a width of 1" (25.4 mm) was cut from the purchased composite panel. Strain gauges were installed on the face of this sample. The gauges used were Vishay Micro Measurements General Purpose Strain Gauges. These were 2 mm resistance strain gauges with a grid resistance of 120.0 \pm 3% Ω and a gauge factor of 2.1 \pm .5%. One was installed at the center in the axial direction, and a second above the axial gauge in the transverse direction. The alignment of the strain gauges is shown on the left side of Figure 6.

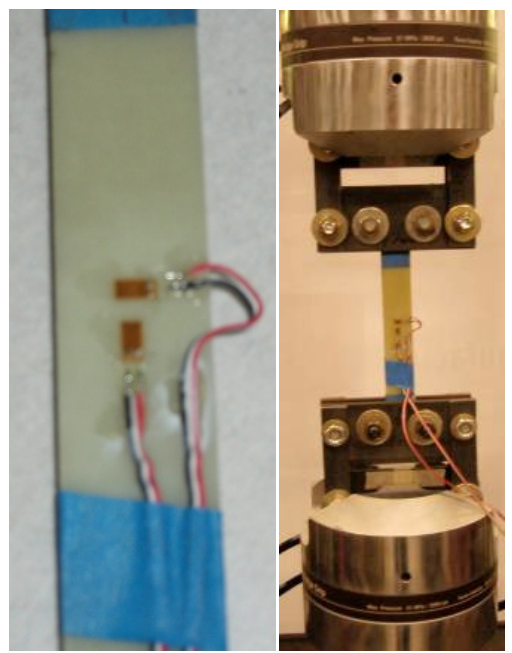


Figure 6: Strain gage placement and installed specimen.

This sample was tensile tested in the MTS 810. The specimen fixture detailed above was used with no offset in this testing. The sample is centered by spacers and held by friction between 2" (50.8 mm) of material clamped into the top and bottom fixtures. Load from the MTS is transferred via the friction from the specimen clamps. The test was then setup in the MTS station manager software.

The MTS station manager software allows for a variety of test parameters to be controlled. For tensile testing, displacement of the head is specified, and time displacement and force are recorded. The displacement of the head was specified to be a ramp at the rate of .5mm per minute or (.02"per minute). The quantities of Time(s), Displacement (mm), and Force (N) were measured and recorded by the software at a rate of 1 record every .1 second. This data was outputted into a file.

The readings from the strain gauges are measured on a separate computer using the Labview software with a specially designed program. This program computes the strains based on the signal from the gauge and the gauge factor. Then the software records values of micro strain at a specified rate. This rate is chosen to be comparable to the measurement rate of the MTS software.

Using the two files containing data produced during the test, the data is synced and analyzed. Using the Force measured in the MTS software and cross sectional area of the specimen, the stresses during the experiment are found. These stresses were then plotted against the strain recorded from the gauges. The resulting graph is used to calculate the slope of the curve to determine Young's Modulus. One of these plots is displayed below in Figure 4. The Poisson's Ratio is determined in a similar way as the ratio of the Axial Strain and the Transverse. The plot for Poisson's ratio is shown in Figure 5. Values determined by this experimental testing are listed below in Table 1.

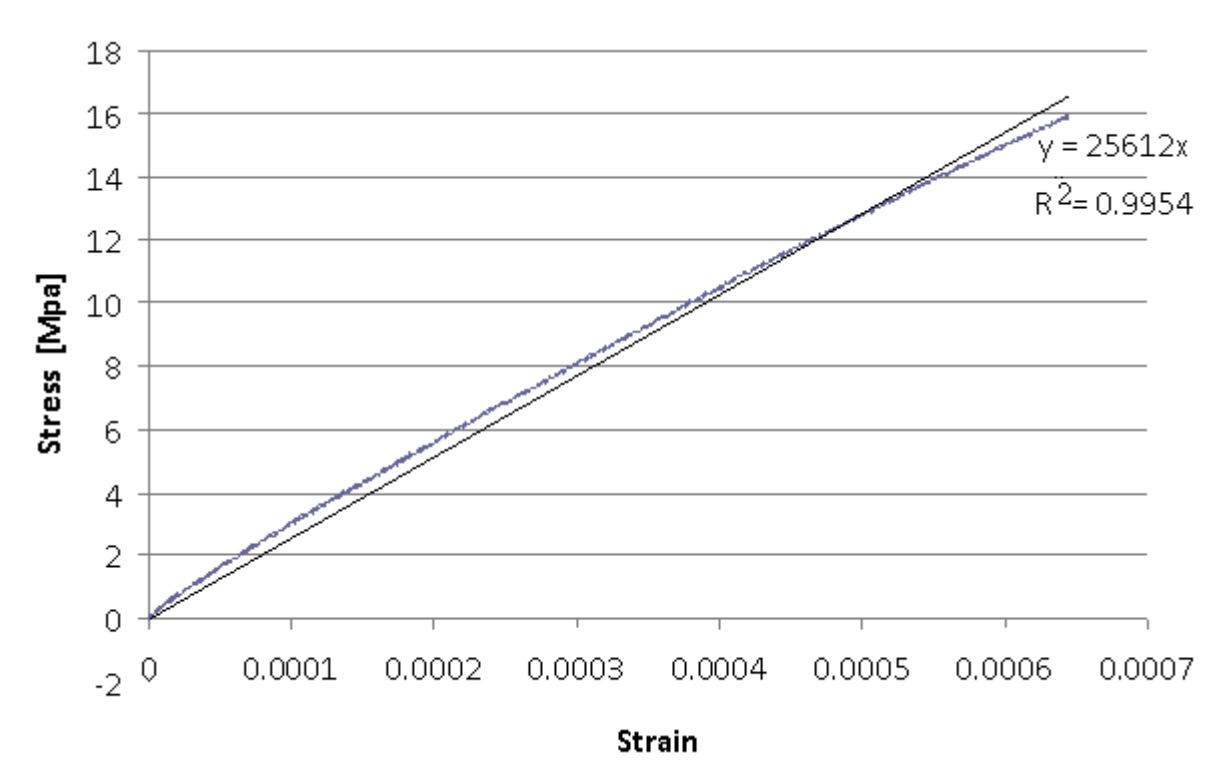


Figure 7: Stress is plotted against strain measured by the gages.

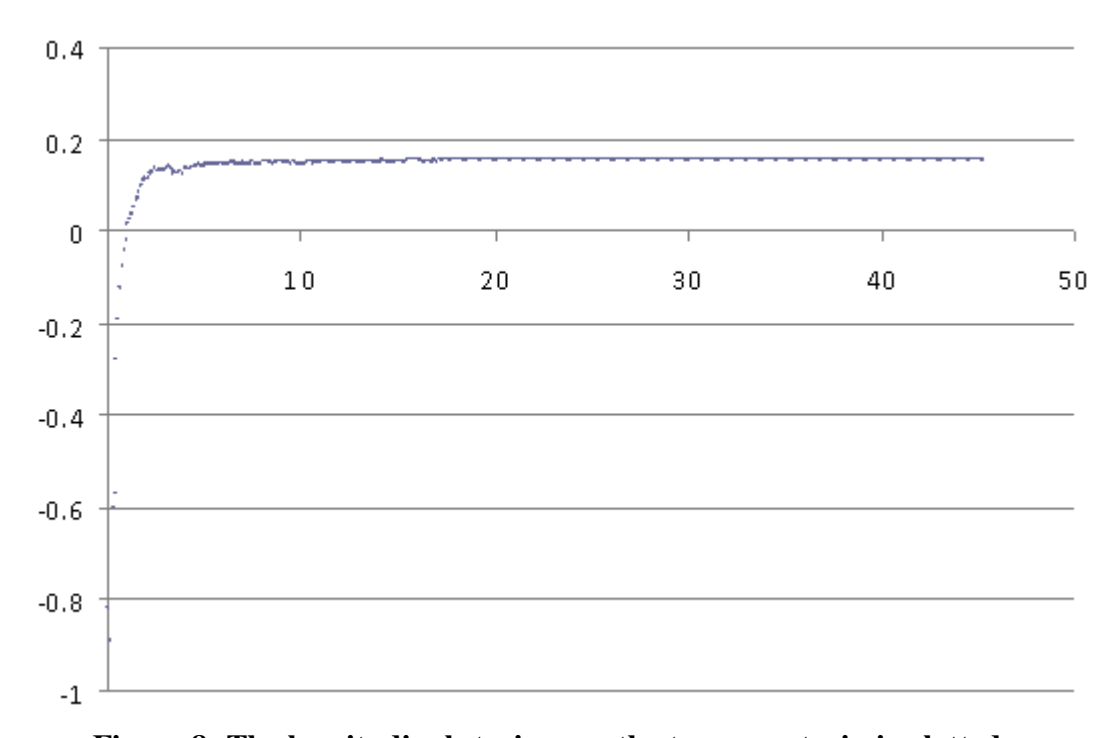


Figure 8: The longitudinal strain over the trnsvers strain is plotted.

Table 1: Experimentally determined material properties of G10 Garolite.

Young's Modulus E	Poisson's Ratio <i>v</i>	
25612 MPa	0.155	

Initial Destructive Testing

Preparation of the samples consisted of only machining processes. The samples are cut in a band saw from the larger panel. The samples are cut to the size of 4" x 8" (101.6 x 203.2 mm). The width of 4" (101.6 mm) was decided upon to ensure that premature failure from net tension would not be experienced during testing. The length of 8" (203.2 mm) was picked so that the optimum number of samples would be extracted from a single panel. After the samples were cut, the holes were drilled in a mill to ensure accurate positioning. The location of the center hole was chosen to have a ratio of diameter to edge distance of 4; this ratio has been shown to exhibit bearing failure. Bearing failure is ideal because it has the highest yield strength compared to other joint failure modes. A completed sample is shown in Figure 6.

To ensure problems do not arise due to St. Venants effect, a finite element study was performed with a colleague. The study is performed with the boundary conditions proposed for the current study. Strains are then observed from the boundary along a line to the bottom of the hole of interest. These results are shown in Figure 6. From these results, the strains can be seen to level out for each of the lengths. Thus the length of 4.675" (118.75 mm) will not affect the results at the hole of interest.

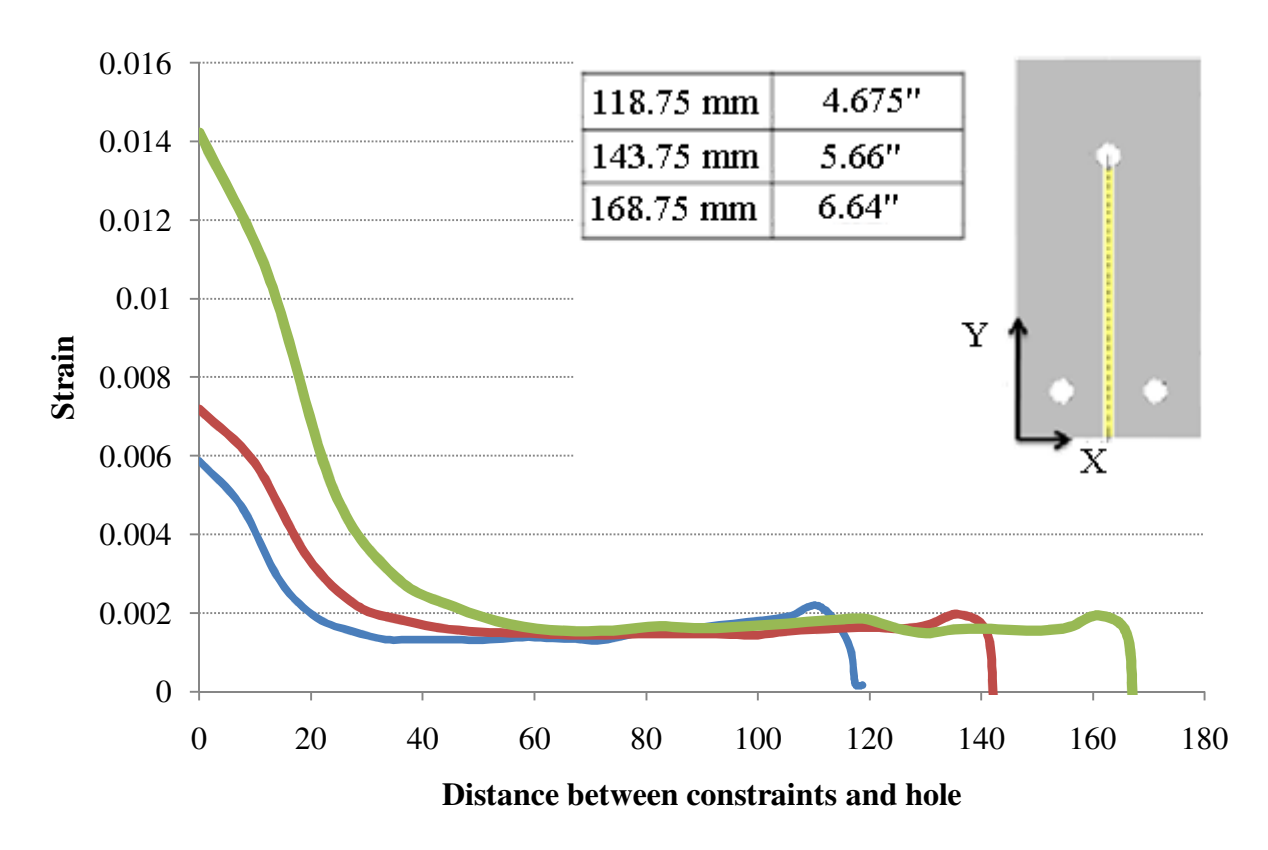


Figure 9: FE analysis for St. Venant Effects.

For the destructive testing, no external or internal gauges were installed on the samples. The only measured readings were the time, displacement, and force recorded by the MTS software. The specimen fixture detailed above was used with an offset to allow for a single lap shear test. The samples were centered by the spacers at the side and bolts connected the sample to the fixture. Load from the MTS is transferred via the bolts through the specimen clamp and sample. An aluminum plate was used as the second plate in the lap joint. It was connected to the sample by a bolt torqued to 25 in lbs (2.82 Nm). The torque was kept constant at this value based on the recommendation from [5]. This configuration is shown in Figure 7. The test was then setup in the MTS station manager software.

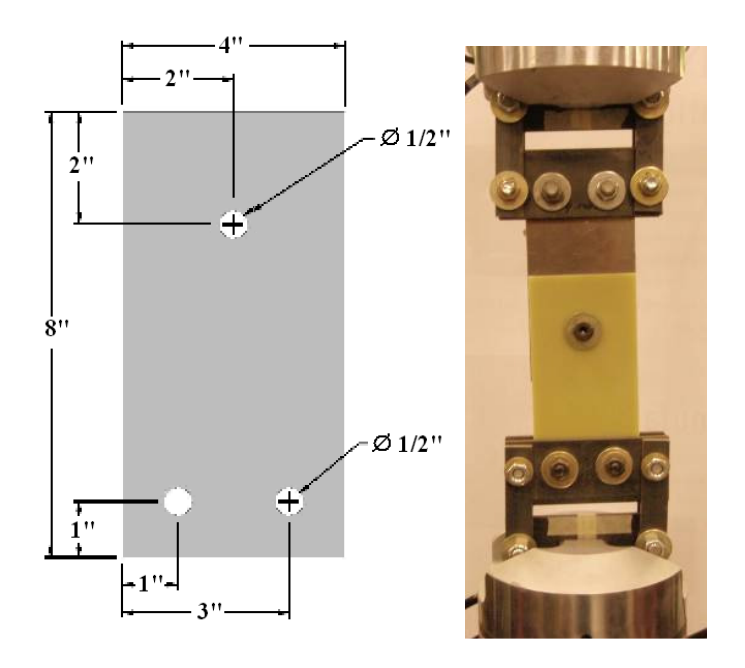


Figure 10: Sample dimentions and test configuration for single lap shear joint tests.

For destructive testing, displacement of the head was specified, and time displacement and force were recorded. The displacement of the head was specified to be a ramp at the rate of 1 mm per minute. The quantities of Time(s), Displacement (mm), and Force (N) were measured and recorded by the software at a rate of 1 record every .1 second.

Baseline Destructive Testing Results

Initial testing was carried out with some difficulty. For multiple tests, the graph displayed by the MTS software consistently showed a flat line in the force being transmitted through the specimen. This flat line would normally be a characteristic of failure, but after removing the specimens, no failure could be seen in the sample. First the problem was purposed to be a failure in the mounting fixture. But this was ruled out when a plate of .25" (6.35 mm) steel was loaded into the MTS and experienced the same results at 30 kN. The problem was then deduced to be a low pressure setting in the hydraulic control box connected to the Grips. The pressure was

increased from 500 psi to 1000 psi (3.45 to 6.89 MPa). Then the steel plate was tested again and shown to reach loads of over 65 kN. With this problem solved, testing continued.

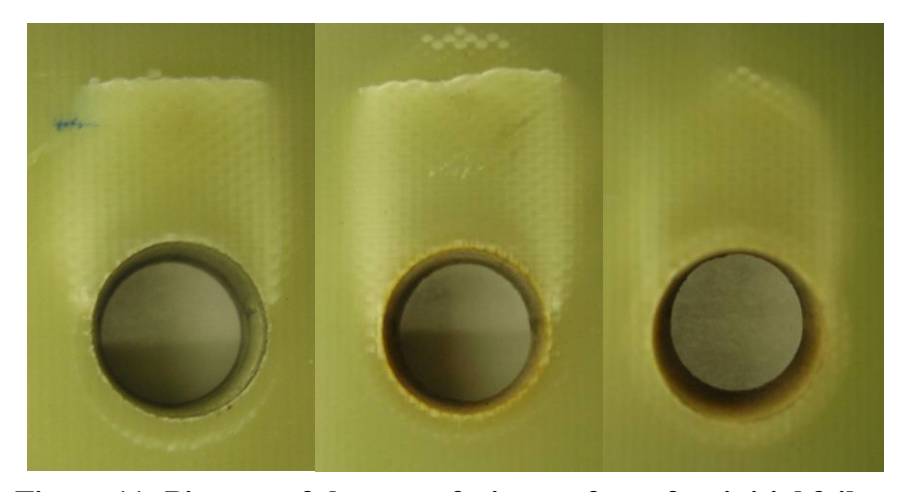


Figure 11: Pictures of the outer facing surface after initial failure.

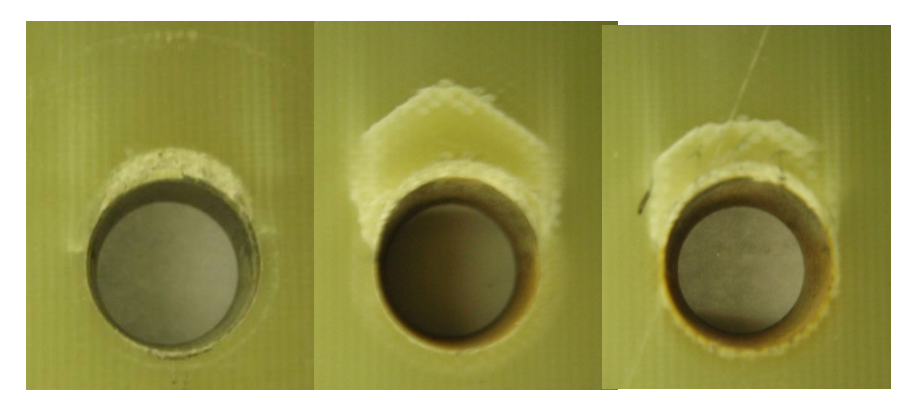


Figure 12: Pictures of the interface surface of the composite after initial failure.

From Figure 11, it can be seen that the failure of the joints starts at the interface and continues through the thickness to the outer face. Delamination begins to expand horizontally through the samples after the fracture occurs. In Figure 12, the back of the panel is seen. This side of the panel experiences more direct damage because the bending of the bolt increases contact and causes fiber buckling.

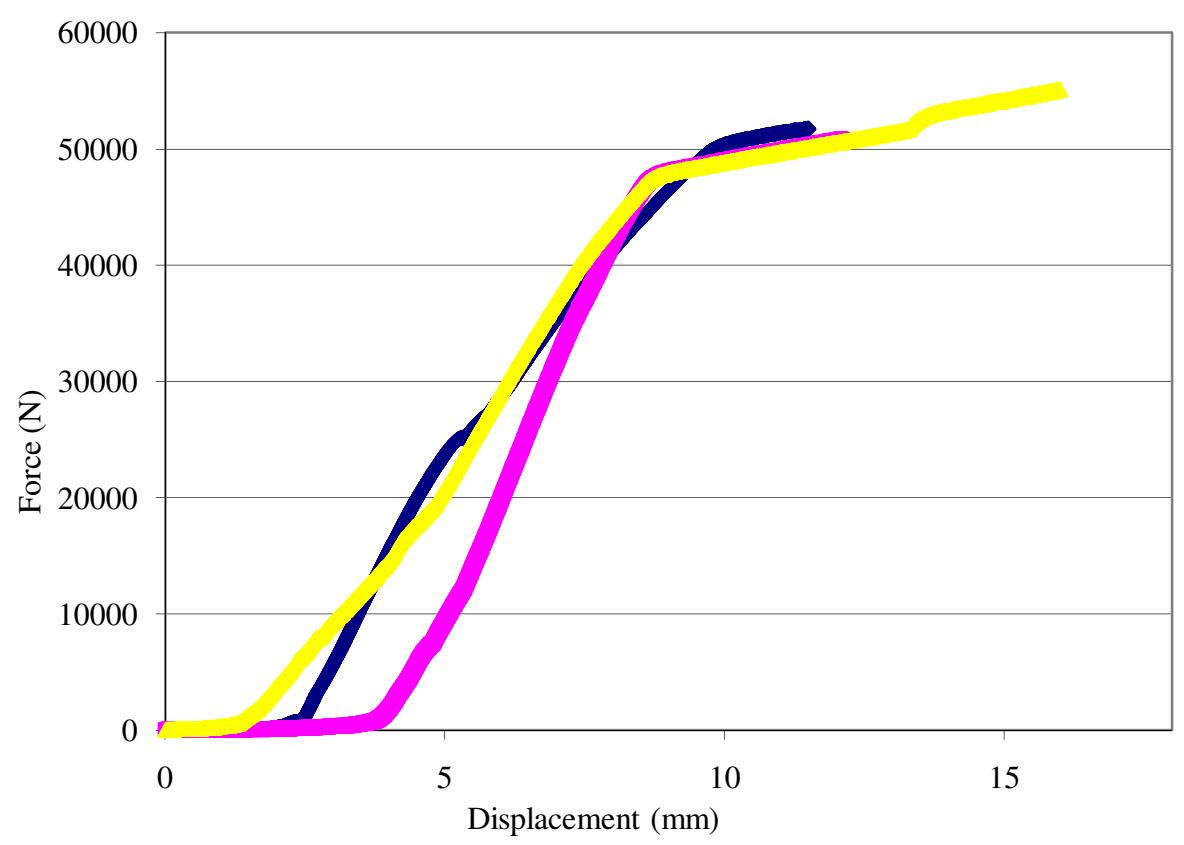


Figure 13: Graph of force vs. displacement for initial tests.

From Figure 13, two problems with the testing were seen. The first was slipping in the grips was occurring. This can be seen in the graph where the sudden change in slope is displayed at the top end. Due to this assumption the pressure in the control box was increased to 2000 psi to ensure that no slipping would take place. The second problem was the long and varied settling of the joints in the fixture. These are the very low forces at the beginning of the graph before an upward slope was established. The problem was proposed to be the movement of the crosshead prior to the test. The command while inserting the fixture was to maintain 0 N of force, but this caused the cross head to compensate and create slack in the joints. To help eliminate this problem, the MTS software was set to maintain 0 N of force while initially gripping the fixture. After the sample was secure and force was zeroed, the command to stop all displacement was selected.

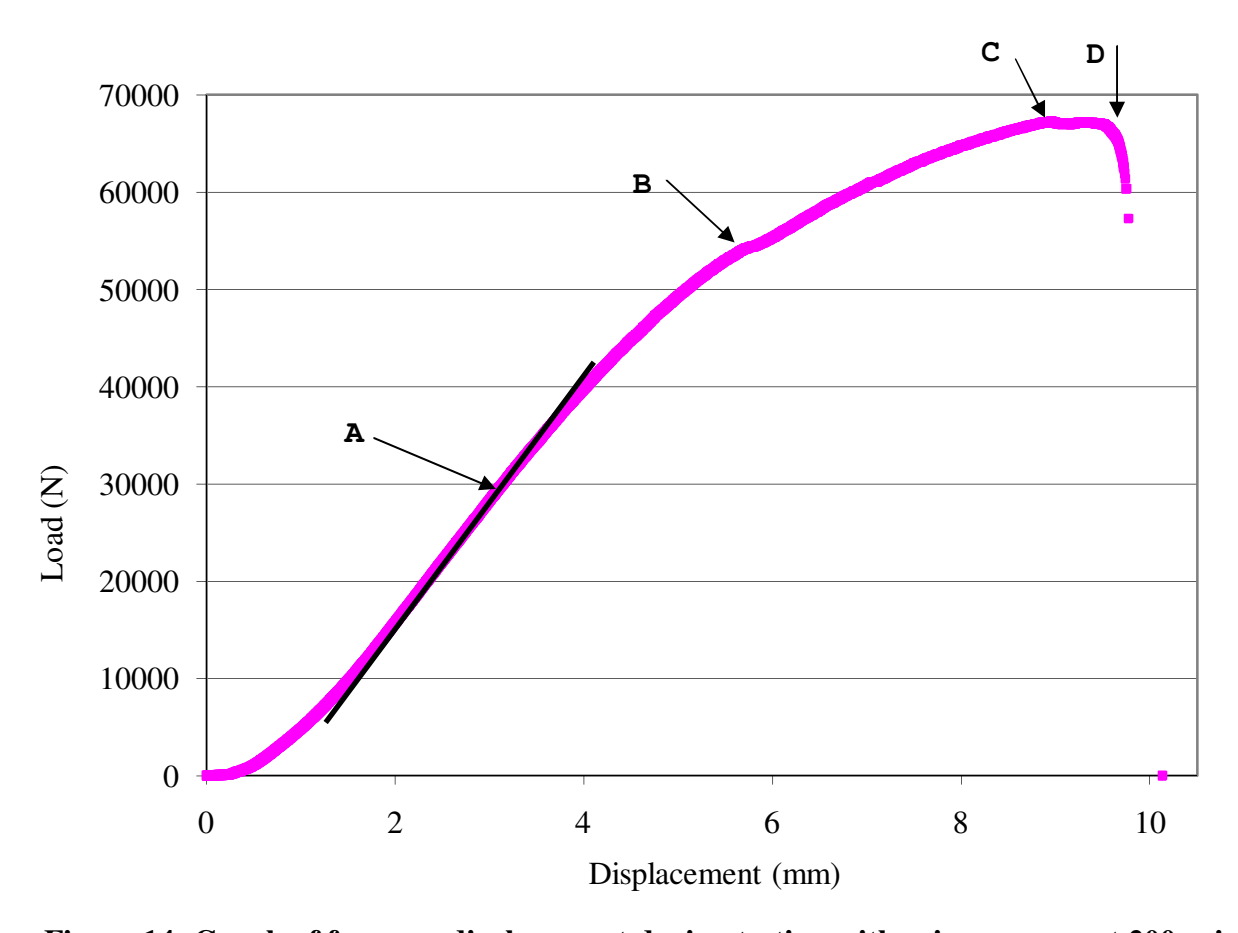


Figure 14: Graph of force vs. displacement during testing with grip pressure at 200 psi.

Results from experiments run with the higher pressure can be seen in Figure 14. As can be seen from the graph, the test was run to ultimate failure. At point A, the slope deviated from linear. In order to identify the initial failure point, the .02% rule will be used. In order to calculate this point, the slope and intersect are found for this linear range. For these specimens, the gage length is assumed to be 10" or 254 mm. The specified gage length means that for the .02% strain is equal to .05 mm. The regression line is then moved by the .05 mm and this point specifies the initial failure.

This is also when delamination can be seen on the outer face. This delamination can be seen in Figure 15. As the load passes point B, delamination becomes better defined and increases in width. From point B to C, the delamination continues to progress and after C the fibers begin

to fail in the form of net tension. The ultimate failure occurs at point D where catastrophic net tension failure takes place.

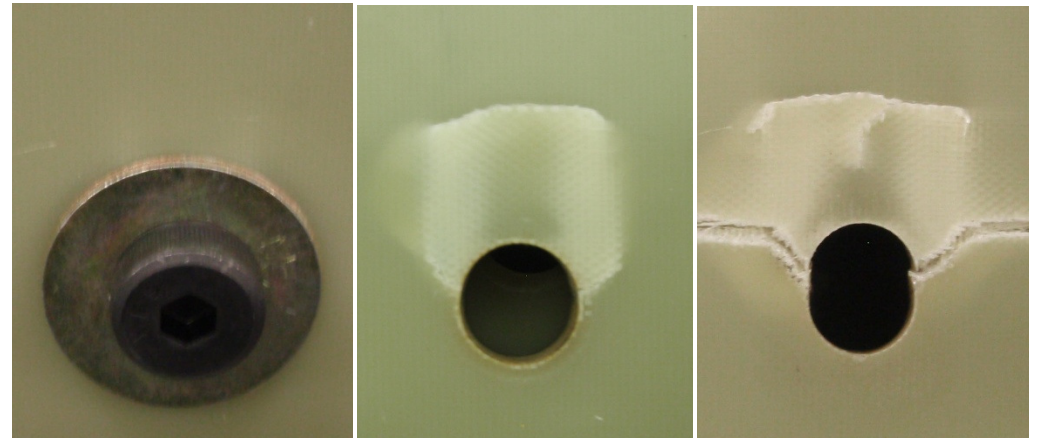


Figure 15: Pictures corresponding to Points A, B and D in Figure 14.

This failed specimen was then bisected. The bisection allowed for the failure through the thickness to be seen, as shown in Figure 10. From this view, delamination and fiber failure propagated at a 45° angle. The failure started at the edge of the hole in contact with the aluminum plate. This point was subjected to the highest stresses because both the bending and the bolt act on that point. The failure propagation is seen in Figure 16 as the section between point A and B. At point A, the first failure began, this continued until the crack broke through the outer face at point B. It is believed that this failure through the thickness did not have significant effect on the final net section failure but did alter the load carrying capacity of the plate. With these latest results the testing process has been refined and has given reliable results.



Figure 16: Bisection of failed specimen.

Layered Test Samples

As has been shown in previous literature, increasing the thickness of composites decreases the strength. These decreases can be caused by increased chance of voids and imperfections, ply misalignment, and stress gradients through the thickness. In an effort to see the effects of using .5" thick samples, .5" panels are created from layering thinner panels and then tested.

In the current study, the tests are performed with layer thicknesses of .125", .25" and .5". To produce the .5" panel, the contact surfaces are initially sanded and then adhesively bonded with an epoxy. The panel is then clamped and allowed to dry for 24 hours. After the samples are dry, the holes are all drilled to the same dimensions as the baseline.

Once the samples are prepared, they are loaded into the fixture and the preload applied to the joint is 500 N. The test is then performed in the same way as described above for the baseline tests. Key values from the tests are displayed in Table 2 and the results are displayed in Figure 5.

Table 2: Key values for layered specimen tests.

Layers	Stiffness (kN/mm)	Failure Load (kN)	Ultimate Stress (MPa)	Bearing Stress (MPa)
1	10.4	71.0	62.9	440
2	9.6	55.8	49.4	346
4	8.9	50.4	44.6	312

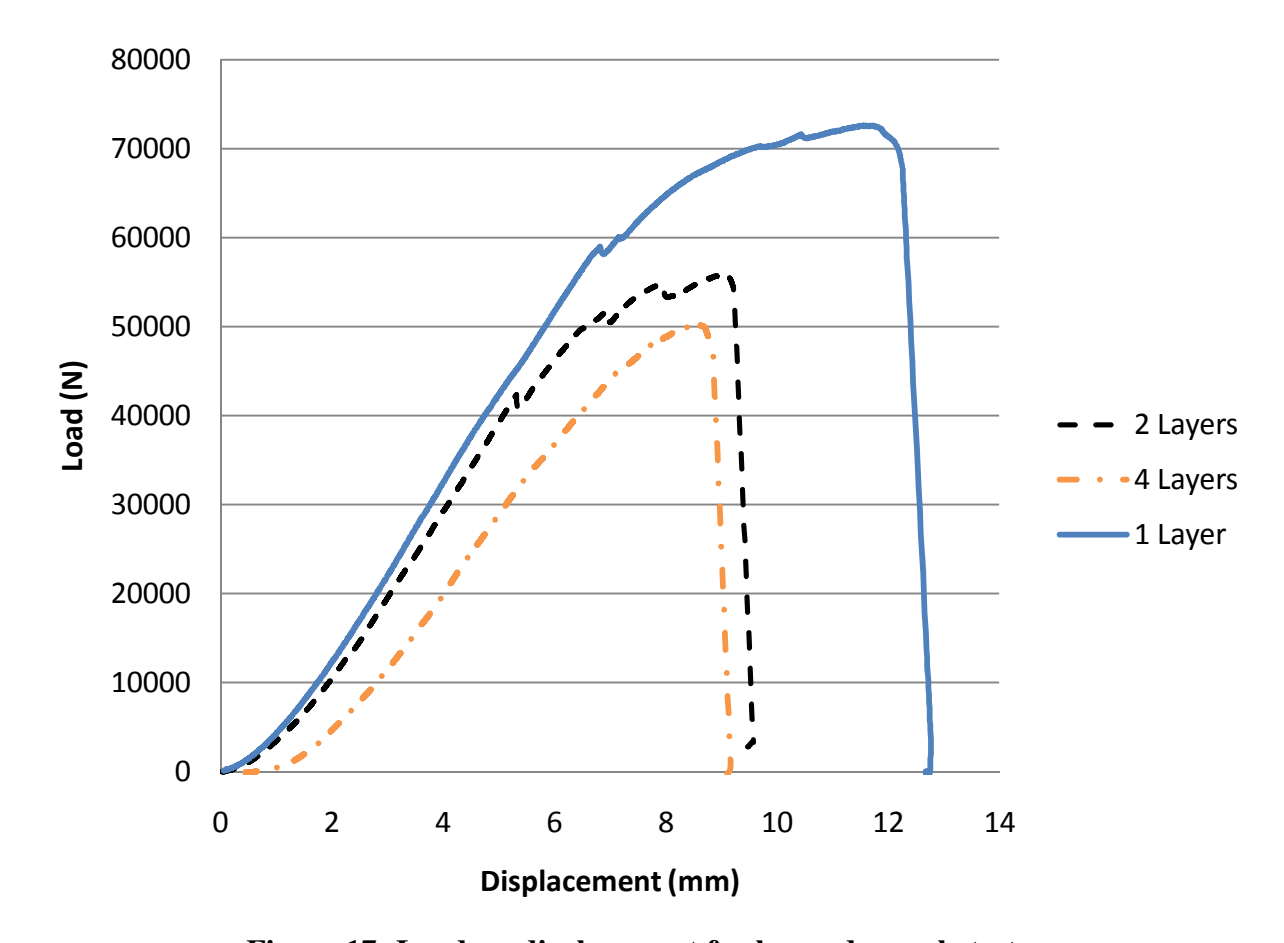


Figure 17: Load vs. displacement for layered sample tests.

From the layered tests, an advantage can be seen in using a single thick layer in the single lap joint configuration. The results show an increase in the stiffness and the failure load. The increase may be because of the shear being better transmitted. This result is attributed to the thickness constraint that also causes the net section failure.

CHAPTER 3 INSERT TESTING

Materials

To test the effects of inserts, composite samples were produced with different hole diameters. For a point of comparison, isotropic inserts were prepared and tested in the same configuration as the Figure 18. Four different inserts were produced, two different sizes and two different materials. All of the inserts were machined to fit a .5" (12.2 mm) bolt and sit flush in the hole of the lap joint. The outer diameters of the inserts used were .625" (15.9 mm) and .75" (19 mm). For materials, Aluminum E = 71.7 GPa and Steel E = 210 GPa were chosen to give the joint either a ductile with the aluminum or stiffer reaction with the steel.

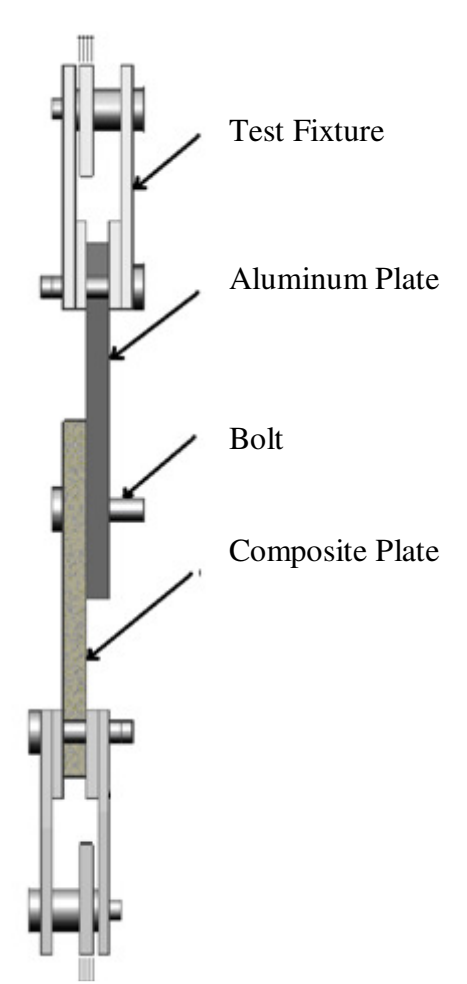


Figure 18: Side view of single lap joint in testing Figure.

For the novel insert design, an insert is formed by injecting a liquid into a fastened single lap bolted joint using a specially designed injection bolt. The liquid is then allowed to cure until a soft insert has formed. The injection bolt is a standard grade 8 hex bolt that has been machined so a liquid can be injected through the bolt into the joint. Figure 19 shows the schematics of such a design; the grayed area represents the injection channels.

Three different designs were initially developed. The first design contains two thruchannels. The channels are perpendicular to each other and are equally spaced through a 1" (25.4 mm) length. The second design contains one thru-channel; centrally located within the 1" (25.4 mm) length. The third design contains two half-channels; the channels are parallel to each other and are equally spaced through a 1" (25.4 mm) length. The channels of all three designs are 0.125" (3.17 mm) in diameter. A length of 0.25" (6.35 mm) of the vertical injection channel has been enlarged to 0.1875" (4.76 mm) to accommodate the injection device. In testing, after epoxy has been injected into the joint, the injector will be removed from the bolt.

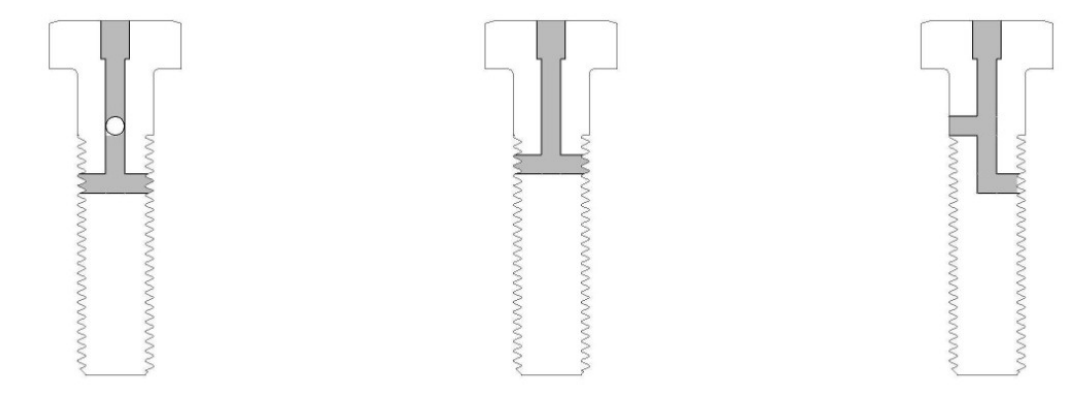


Figure 19: Possible novel insert designs.

A disposable 1oz (30 ml) syringe with a tapered nozzle was chosen as the best option for injection of the resin. The bolts were centered in the holes with clearances of .125 in (3.12 mm) and .25 in (6.35 mm). The samples were then clamped and torqued to 2.5 in lbs (2.82 Nm). The

dual thru-channel bolt was chosen for testing because it would allow for the fastest injection of the resin with the least amount of voids. After the setup was tightened the thin epoxy resin was injected into the bolt.

Insert Testing Results

The following are the results from the experiments run to failure. As can be seen from the Figure 20, the baseline tests were run to final catastrophic fiber failure with just a simply bolted lap joint. The graph begins as non linear as the slack is removed from the fixture. The initial building of load remains linear between 10 and 35kN; from these regions the stiffness of the joint is calculated. Again after the initial failure, delamination grows until final catastrophic failure.

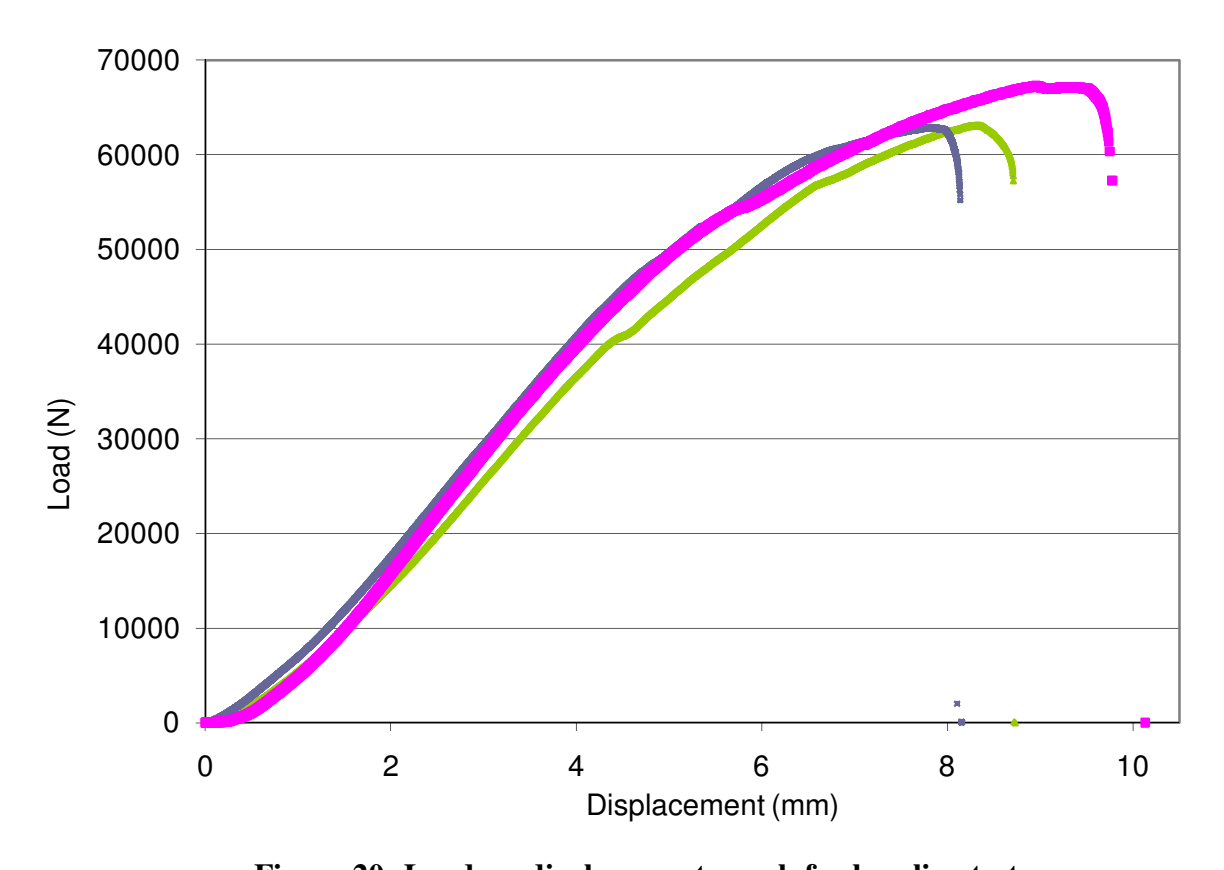


Figure 20: Load vs. displacement graph for baseline tests.

Testing for the inserts continued in the same setup as the baseline tests. Results from the isotropic inserts are shown in Figures 21 and 22. Inserts with an outer diameter of .625" are displayed with a dashed line and the results for the .75" outer diameter are shown as solid.

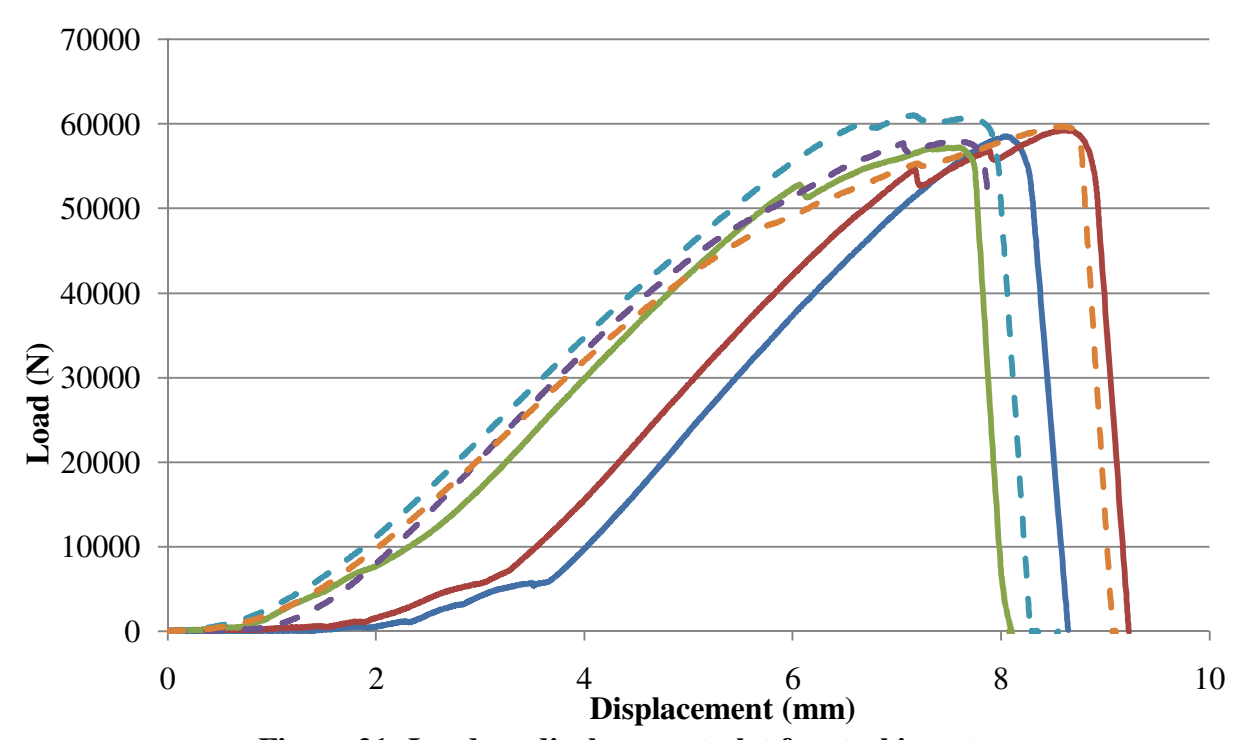


Figure 21: Load vs. displacement plot for steel inserts.

Notice that the stiffness of the joint increases with the increased amount of material in the isotropic inserts. This trend is in both the steel and aluminum tests. For each OD, the steel produces the highest stiffness. Ultimate load however does not change drastically

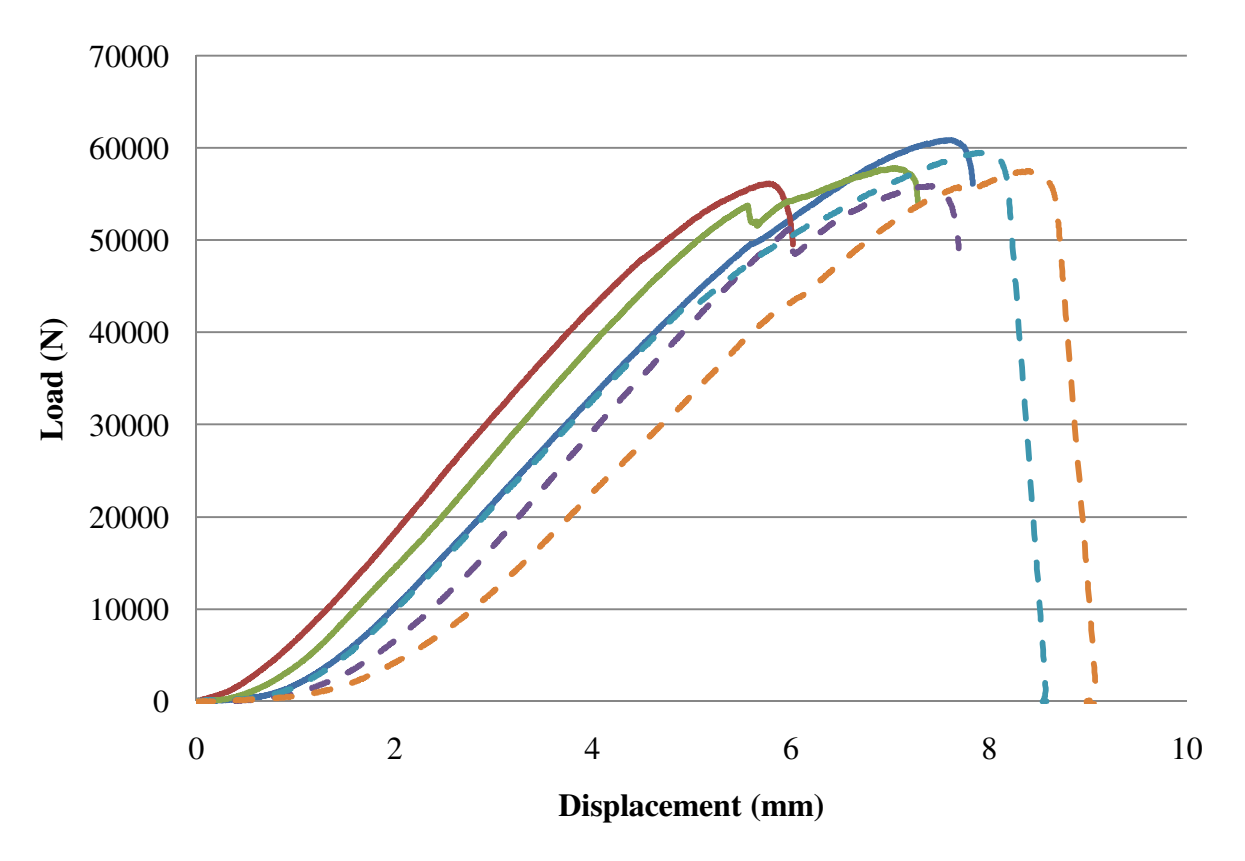


Figure 22: Load vs. displacement plot for aluminum inserts.

From the data provided during testing, several values were calculated for each test.

Averages are presented below in Table 3.

Table 3: Key values from insert testing.

		Initial Failure	Ultimate Load	Bearing Stress
	Stiffness	(kN)	(kN)	(MPa)
Base	9771	33.4	64.8	402
AL625	11500	41.7	57.6	238
AL75	12316	40.7	58.3	181
ST625	12173	37.6	58.6	242
ST75	13737	38.8	58.3	181
Novel 625	15464	NA	NA	NA
Novel 75	15637	NA	NA	NA

It is important to note that the novel bolts failed at approximately 45kN. This failure occurred along one of the grooves as shown in Figure 23. As also shown in Figure 23, the resin

had failed. The resin failing created an impulse which caused the bolt to fracture. This is why there is no data provided for these inserts in Table 3.

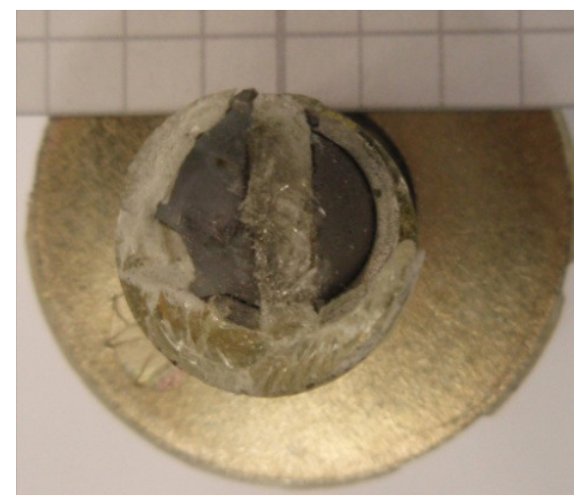


Figure 23:Cross section of failed novel insert.

CHAPTER 4 NOVEL PRELOAD SENSOR AND PRELOAD TESTING

Preload Measurement Techniques

Many manuals and textbooks have techniques for measuring preload. Several, as described in Budynas et al(2006) and Bickford (1995) do not require specialized tools. The simplest way to determine the amount of preload on a joint is the use of a measuring device to determine the elongation of the bolt. Using the elongation, the preload can be calculated because as in a tensile specimen elongation is linearly related to the amount of load seen in the bolt. Expressed in Equation 1, the preload (P) is found using the cross sectional area of the bolt (A), the bolts Young's modulus (E), the deflection (d) and the overall length of the bolt (L).

$$P = \frac{AE\delta}{L} \tag{1}$$

Because of variance and inaccuracies associated with manual measurement errors have been found to be within a range of \pm 5%.

Using the same concept as measuring elongation, some will manually stretch the bolt and then secure it in that state by installing the bolt. The bolts can be stretched by either directly stretching or heating the material to the desired length. This process is normally done on large fasteners as it is difficult and often dangerous to install or remove such joints.

Often times however, both sides of the joint are not easily accessible making highly accurate measurements extremely difficult or impossible to obtain. The following techniques do not require the user to measure the elongation. One simple technique is the turn of the nut method. Once the nut has been applied and firm contact exists, using additional turns of the nut will produce the desired tension. This method can only be used when the parameters of the joint are known because the calculations will vary. Normally the correct preload with this technique

must be first experimentally determined because different surfaces will vary any pure calculations. This method results in errors of approximately +/- 15% when the proper calculations are made because the variation between bolts.

Another simple technique and the most common to approximate the preload is using a Torque wrench. The joint is assembled and then the nut is tightened with a torque wrench. The torque wrench will indicate the torque being applied to the joint. Note that the values of torque measured are normally found to be highly variable. From the designated torque (T), the preload can be determined by dividing the torque by the product of the torque coefficient (k) and diameter of the bolt (D).

$$P = \frac{T}{k * D} \tag{2}$$

The values for k are determined based on thread geometry, coefficient of friction on the threads, and the collar coefficient of friction. These values can be found in tables but will vary from bolt to bolt because of cleanliness or variability in the coatings. Between the variability of the measured torques and the inaccuracies in the torque coefficient, this technique is the least accurate. Errors therefore have been seen from the torque calculation as high as +/- 25%.

One method to reduce the inaccuracy of applying a preload with a torque wrench is to use yield control. This method uses a more advanced torque wrench that is able to measure the torque gradient. When changes in the torque gradient occur, as shown in the yielding point in Figure 24, the wrench indicates that yielding of the bolt has begun. The torque is then removed and the bolt settles at approximately its yield point. Similar fasteners will yield at a known loading, so that loading is then used to calculate the preload in the joint. Although the loads are consistently applied, the disadvantage of this technique is that only one preload can be accurately

applied. Fortunately in most applications the maximum preload is desired and this method is able to provide consistent results.

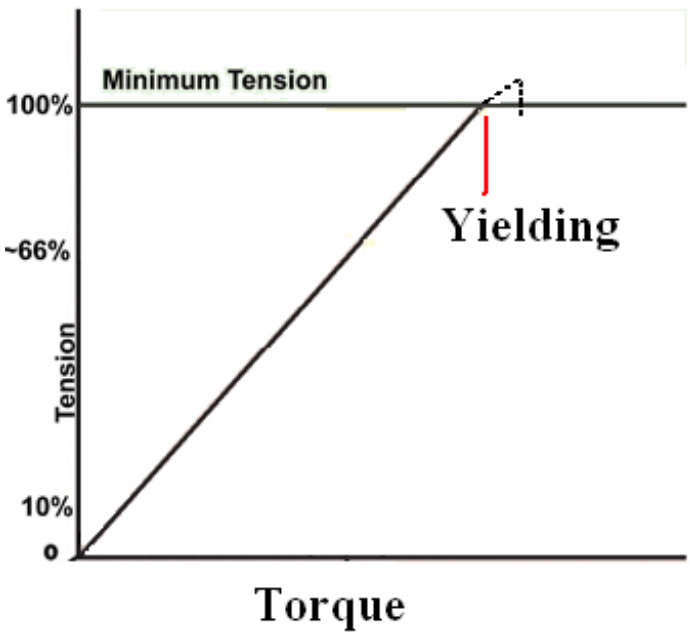


Figure 24: Torque Control Curve

A specialized method for determining the preload in the joint is a Direct Tension Indicator washer. These special, single use washers, example shown in Figure 25, are produced with feeler gages on the surface. These feeler gages are designed to crush at predetermined load. Thus use is simple, once the desired preload is specified the correct DTI washer is placed in the joint and the nut is tightened until the feeler gages on the washer are crushed. While they are not reusable they offer for simple operation and provide errors in the range of +/- 10%.



Figure 25: Direct Tension Indicator Washers

The following methods use advanced techniques to measure the stress in joint or elongation of the bolt. A load cell uses strain gages to measure the deformation of the transducer. The transducer can be placed in the joint. Once the joint is loaded it causes a deformation in both the bolt and the transducer. This deformation in the transducer is then measured as a change in resistance of the strain gages and can be directly related to a preload. These load transducers produce a linear relationship between the amount of deformation and the load. So once calibrated they allow for accurate measurement for different loads. Unfortunately these load cells are often larger adding weight and altering the mechanics of the joint.

A similar method to using the load transducer is to use a Resistance Strain Gage
Instrumented Bolt. This involves creating a hole in the center of the bolt then applying strain gages on the walls of the hole. These gages are normally installed in a full bridge setup. This configuration will remove variations due to bending because these moments will be canceled.

Also an average of the strain can be found producing more accurate readings. The averaged strain can then be found to linearly vary with the application of preload. While this method removes the extra material of a load transducer, there is also a disadvantage as a large amount of material is removed from the bolt weakening it. But once calibrated, both the RSG instrumented bolts and load cells can accurately measure the preload within 1 to 2%.

In Jhang et al (2006), the use of ultrasonic velocity measurement is applied to determine the preload in a joint. This method uses a bolt with both ends precision machined to allow for precise contacts to be made. Shown in Figure 26, an ultrasonic wave is sent down the length of the bolt and its Time of Flight is measured. After the initial TOF is measured the bolt is loaded and the TOF for the loaded bolt is measured. The change in TOF is then used to calculate the change in length. Using the change in length, Equation 1 can be used to a much more accurate

degree because of the precision of the elongation measured. Using a load cell and a torque wrench, this is found to be very linear over multiple tests compared to a torque wrench.

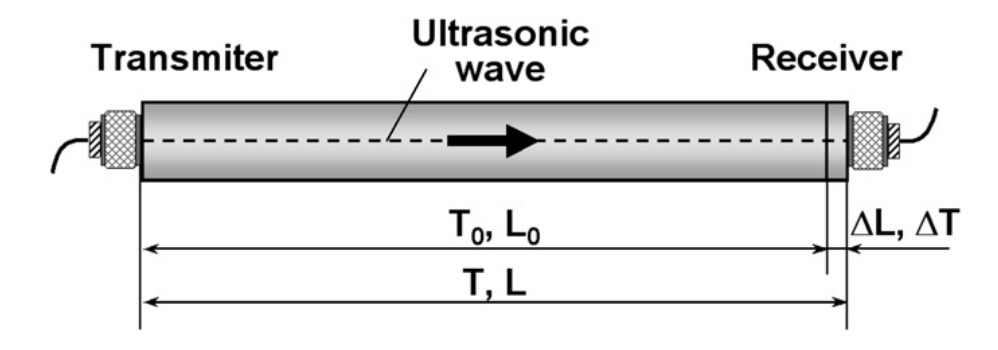


Figure 26: Elongation using TOF

A different technique is proposed in Heyman (1977). Because normal TOF in ultrasonic preload measurements is very susceptible to noise, the tone burst technique is used. The phase detection technique is used to upgrade normal TOF measurement. Like normal ultrasonic measurement, this technique uses TOF to measure elongation but also measures the change in resonance to produce a more accurate strain. Figure 27 details the setup.

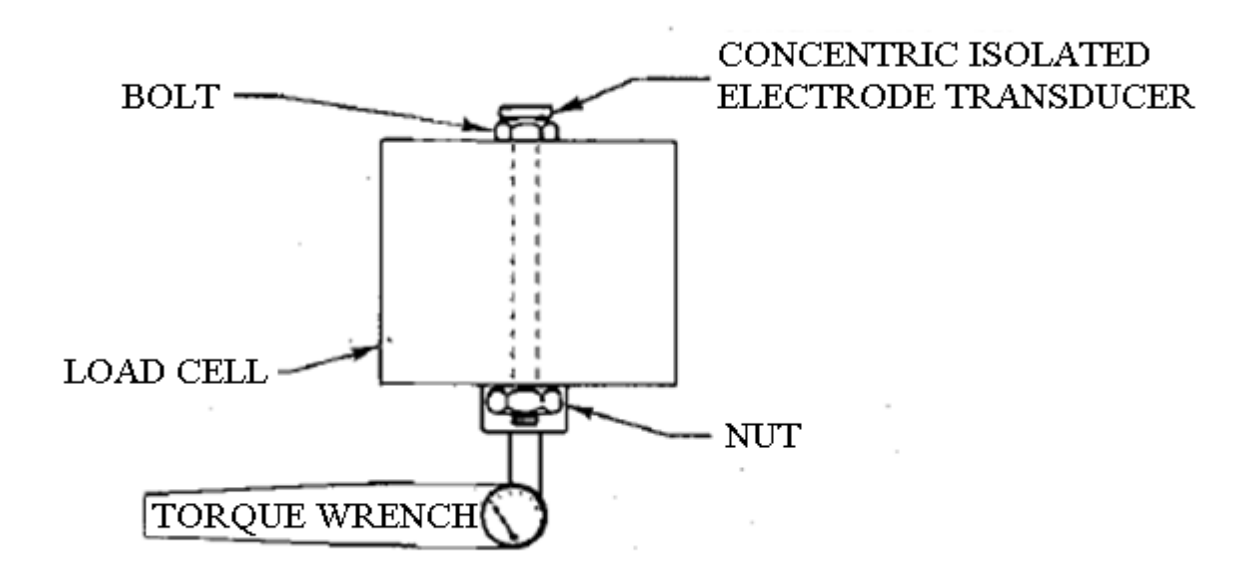


Figure 27: CW Ultrasonic Bolt Experimental Setup

From this strain the same calculations can be made to relate to the preload. Good linear correlation is observed and validates the effectiveness of this technique. The main advantage of this technique is that it does not require precisely machined bolts thus decreasing the cost.

In Nassar et al (2007), Electronic Speckle Pattern Interferometry is used to determine the preload. ESPI is a full field technique that measures accurate displacements in all three directions. For measurement of preload the displacements in the z direction along the AB line in Figure 28 are measured. Measuring displacement in the z direction along this line at different preloads allows for calibration. Once calibrated a linear trend is found. Low end values produce a certain amount of scatter resulting in less accuracy. Above 15 kN however, accuracy increases to +/- 10%. Advantages to this method are that it requires no specialized fasteners and no contact is made with the joint making it an effective tool that could be used in real time. The disadvantage is that this is material specific requiring the calibration of all assembly materials.

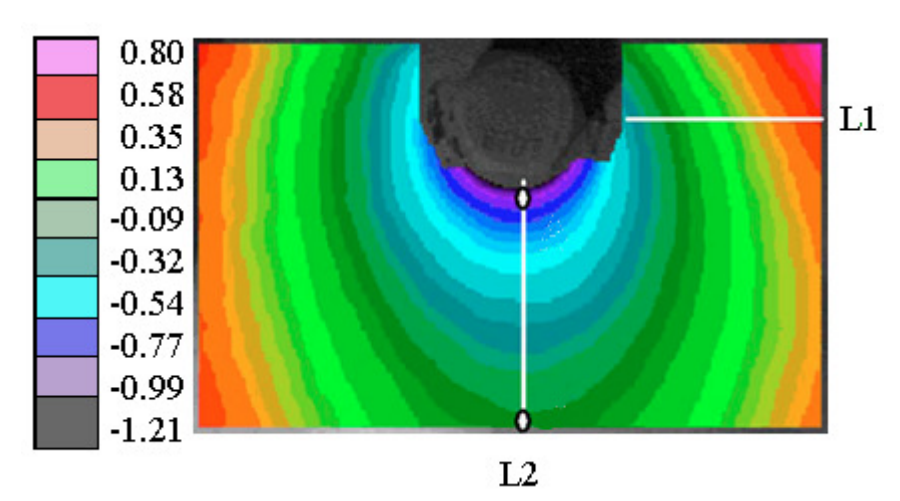


Figure 28: 3D ESPI Image at 26 kN preload

Another full field method for use with measuring preload is Automatic Digital Image Correlation as described in Huang et al (2009). ADIC uses normal DIC with an automatic algorithm that measures deformation on washers similar to the one shown in Figure 29. This algorithm first calculates the average strain in the z direction. Then takes into account the

material properties of the washer and automatically converts the strain to a preload. Because the relation is again linear the program can continuously measure the preload as the strains are found. The experiments preformed showed the maximum discrepancy be +/- 4%.

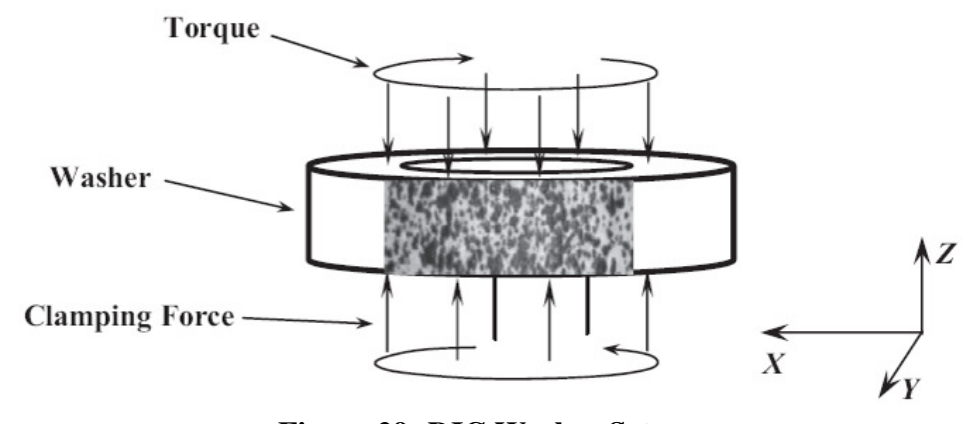


Figure 29: DIC Washer Setup

Much like ESPI, using ADIC does not require contact with the joint, but measures strains in the washer instead of displacements on the surface. This means that once a certain type of washer is prepped for ADIC it can be used with different materials.

Construction of the Novel Preload Sensor

The proposed design will use fiber optic Bragg grating strain gages. Fiber optic gages with Bragg Grating are outlined in Melle et al (1993) and simple application is seen in Kim et al (2004). Fiber optic strain gages consist of an optical fiber with a Bragg grating. The light sent in the core reflects a certain wavelength that adds constructively with each grating. As can be seen in Figure 30, a full range of wavelengths are sent down the fiber and only the wavelength reflected by the Bragg grating is sent back while the rest of the wavelengths are transmitted through the fiber. This reflected light has a certain wavelength which is read by an interrogator.

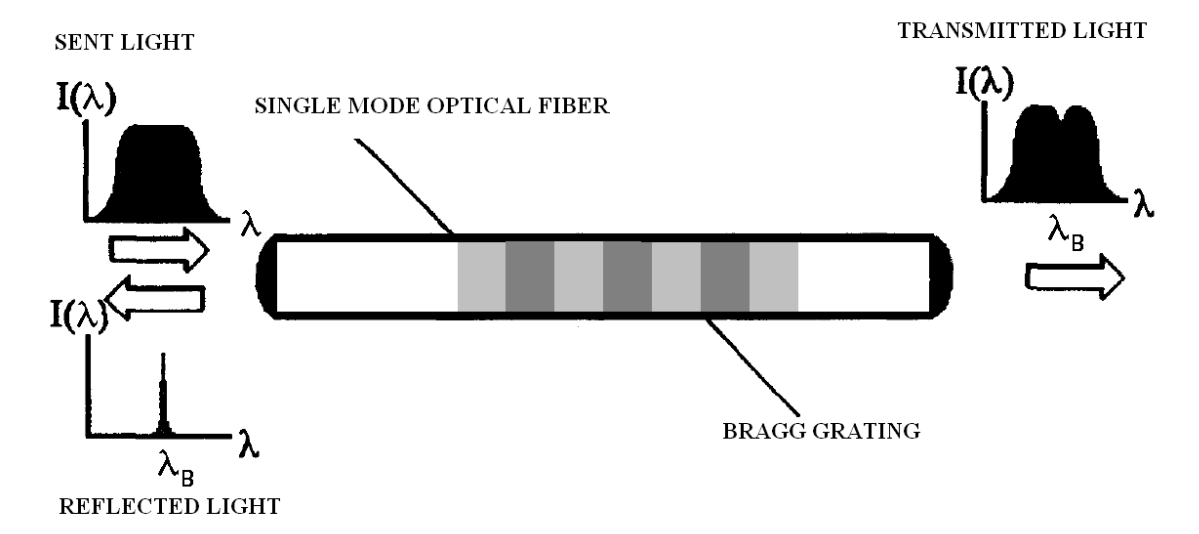


Figure 30: FOSG Operation

The change in wavelength measured can then be related linearly to the strain with a gage factor as shown in the following equation.

$$\varepsilon = \left(\frac{\Delta \lambda}{\lambda}\right) * gf \tag{3}$$

FOSGs are corrosion resistant and have electromagnetic interference immunity, which are some advantages over conventional resistance foil strain gages. They are also smaller meaning that they have less influence on the material than a RSG.

The design of the FOG Instrumented Bolt consists of embedding a FOSG gage in a bolt. The bolt used in the current design is a .5" diameter 3.5" long Grade 8 bolt. These bolts are readily available and have been used in previous tests. They also have excellent yield strength (minimum 150 kpsi) allowing for the high loads present during testing.

The bolt is then precision cut through to the center with a wire width of .3 mm. The cutting operation provides an extremely thin groove as seen in Figure 31. Alternative designs of instrumented bolts use Resistance Strain Gages, requiring more material to be removed. The more material removed creates weaker bolts that are not able to withstand the same loads. The

novel design removes much less material so it will have better strength properties compared to a RSG Instrumented bolt. The EDM cut slot provides ample room for the .15 mm diameter FOSG to fit.



Figure 31: EDM Cut Bolt

The FOSG used in this design is specifically customized for this application. The gage length is 10 mm and the fiber also has a protective coating and a strain relief connector. The gage position is placed so that it will coincide with the shoulder of the bolt. This position was decided upon to provide the most continuous cross section.

To bond the FOSG to the bolt, a general cyanoacrylate adhesive was decided upon. This type of adhesive as described in Shantha (1989) provides a high bonding strength when applied in thin films and a fast dry time. It was also determined that the fragile intersection point between the FOSG and bolt head needed to be protected. For protection, a strain relief connector commonly used in electrical connections was selected.

Once all of the materials were selected and the bolt machined, the construction process began. To ensure a strong bond, both the slot and the FOSG were cleaned with acetone. Then as with application of any RSG the surface of the slot is etched and neutralized with strain gage installation supplies from Vishay. With the bolt prepared for embedding of the FOSG, it is inserted into the specialized installation jig.

The specialized installation jig, as shown in Figure 32, is made of extruded aluminum and 4 bolts. The 4 bolts allow for lateral alignment of the bolt. The opening on the top of the jig is to allow the FOSG to be lowered into the bolt. With the bolt installed in the jig, pieces of foam are used to grip the FOSG. With the FOSG gripped, the slot in the bolt is aligned with the FOSG in the jig.

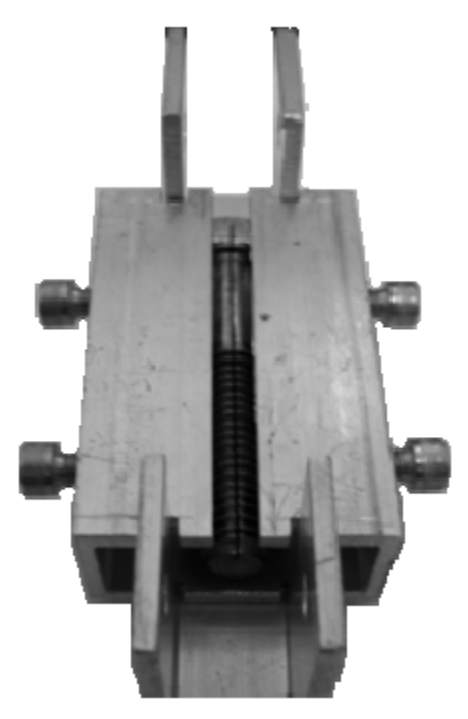


Figure 32: Installation jig for novel preload sensor.

Once aligned the slot and the FOSG are coated with the adhesive. The gage is then immediately lowered to the center of the slot. The gage is fixed in position with the foam and is allowed to cure for 24 hours. After 24 hours, the newly created sensor is removed from the installation jig. Heat shrink tubing and a strain relief cord grip are then applied to the end. The tubing is shrunk onto the end to provide protection to the cable and the grip to limit the bending of the cable in relation to the bolt head. A completed sensor is shown in Figure 33.



Figure 33: Novel preload sensor.

Calibration of the Preload Sensor

With the sensor constructed, the calibration of the sensor is necessary for use. Because the FOSG measures strain based on the change in wavelength, the level of preload can be directly related to the wavelength. Before calibration can begin, the load cell that will allow for calibration must itself be calibrated to ensure correct loads.

The load cell is calibrated by applying known loads and measuring the voltage registered. After several loads are applied, the values are plotted as shown in Figure 34. From this data, the slope is found. This slope is directly related to the amount of load per voltage. As can be seen from the linear regression, the calibration yields a factor of -.0052 N/mV.

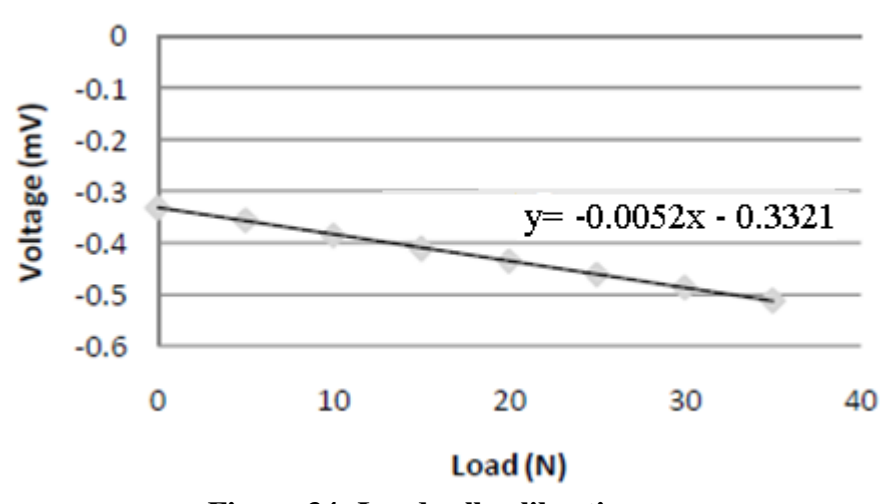


Figure 34: Load cell calibration.

With a calibrated load cell, the yield point of a Grade 8 bolt must be determined. This is necessary in that any testing must be performed within a level that will not damage the new sensor. To determine the yield, the bolt is installed in a joint with a load cell. As preload is

applied, the rotation of the nut and the amount of preload are recorded. The results for two such tests are shown in Figure 35. An observed linear range exists from 1.5 kN to 3.9 kN. For the grade 8 bolt, yield is observed to take place at approximately 4.1 kN of preload.

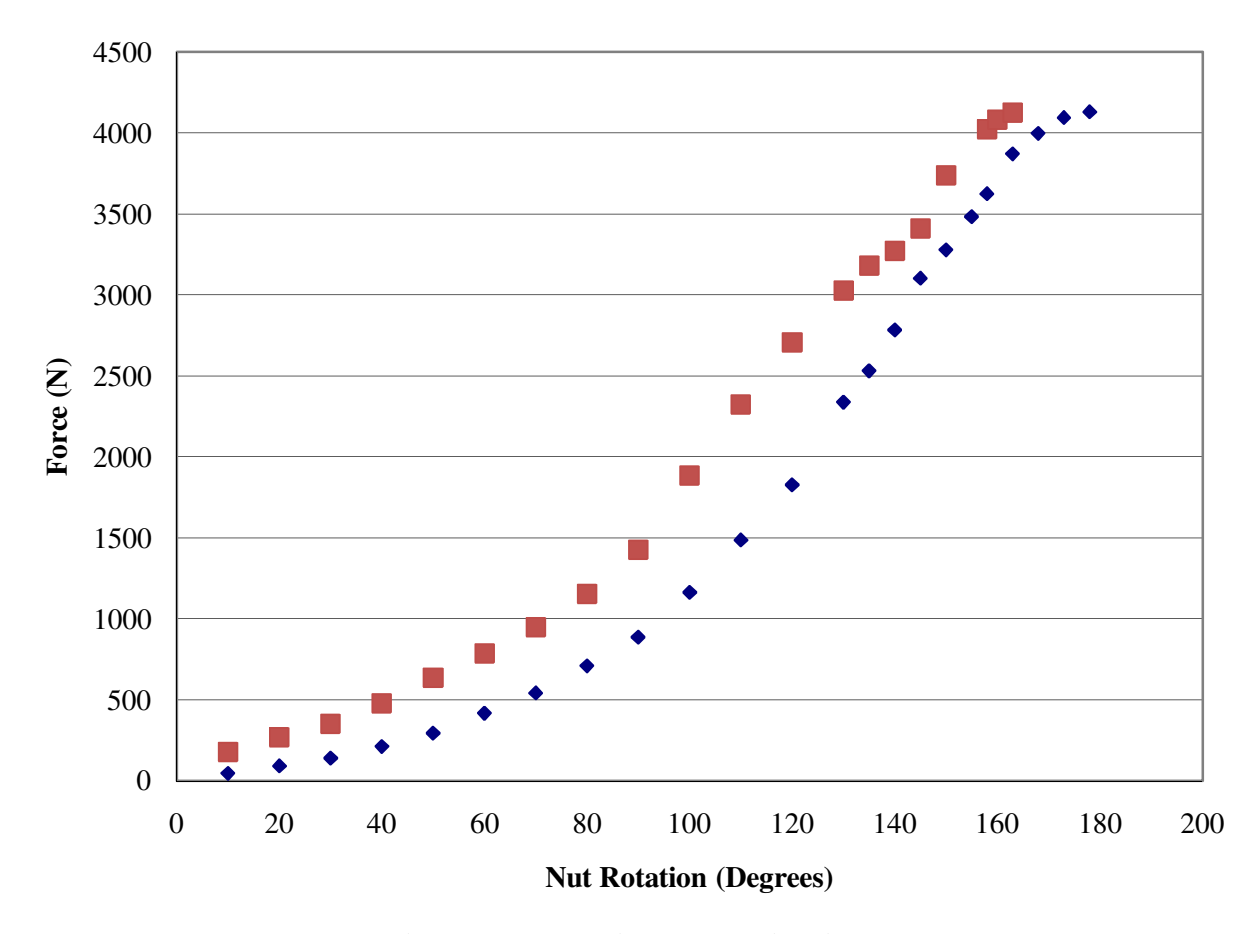


Figure 35: Bolt yield determination.

With the calibration of the load cell and the yield point of the bolts known, calibration of the sensor is to be performed. This calibration could be performed with the use of any of the methods described above. Though using a torque wrench would be the easiest way to apply the preload, unfortunately the scatter in loads based on torque is too high for appropriate calibration. So the load cell has been picked because of its high level of accuracy and simplicity of use.

The first step in calibrating the sensor is assembling the joint with the load cell, as shown in Figure 36. After assembled, the preload is applied by tightening the nut. The preload from the

nut is then recorded along with the wavelengths read from the FOSG. After load is applied at several different levels up to 2200 N of preload, the load is released and the assembly allowed to rest before additional calibrations.

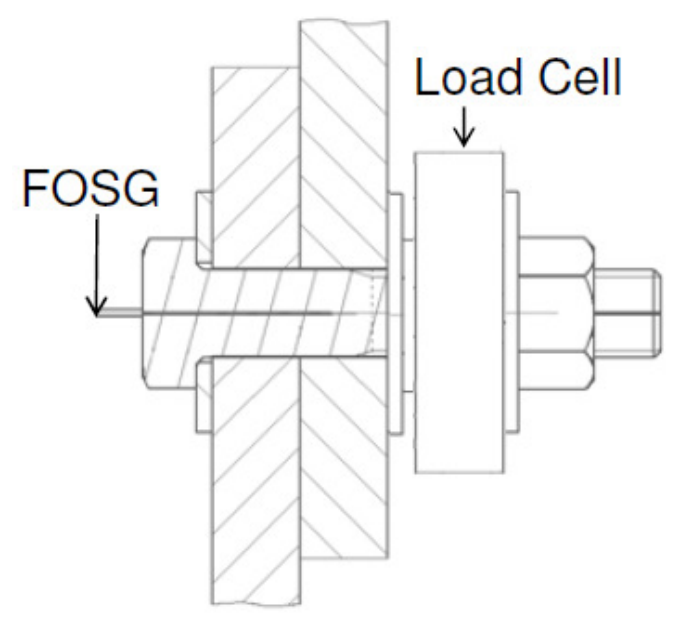


Figure 36: Setup for calibration of the novel preload sensor.

The results from the calibration are shown in Figure 37, with each consecutive set of data points being the following calibration. From the calibrations, the calibration rate is 10.9 kN/nm. This rate has a standard deviation of .680 kN/nm and an average r^2 value of .997. Also, a linear range is observed from 0 to 1200 N. In addition to the loading, the unloading of the calibration is shown in Figure 38. The data shows that the load is not released in a linear fashion and holds strain.

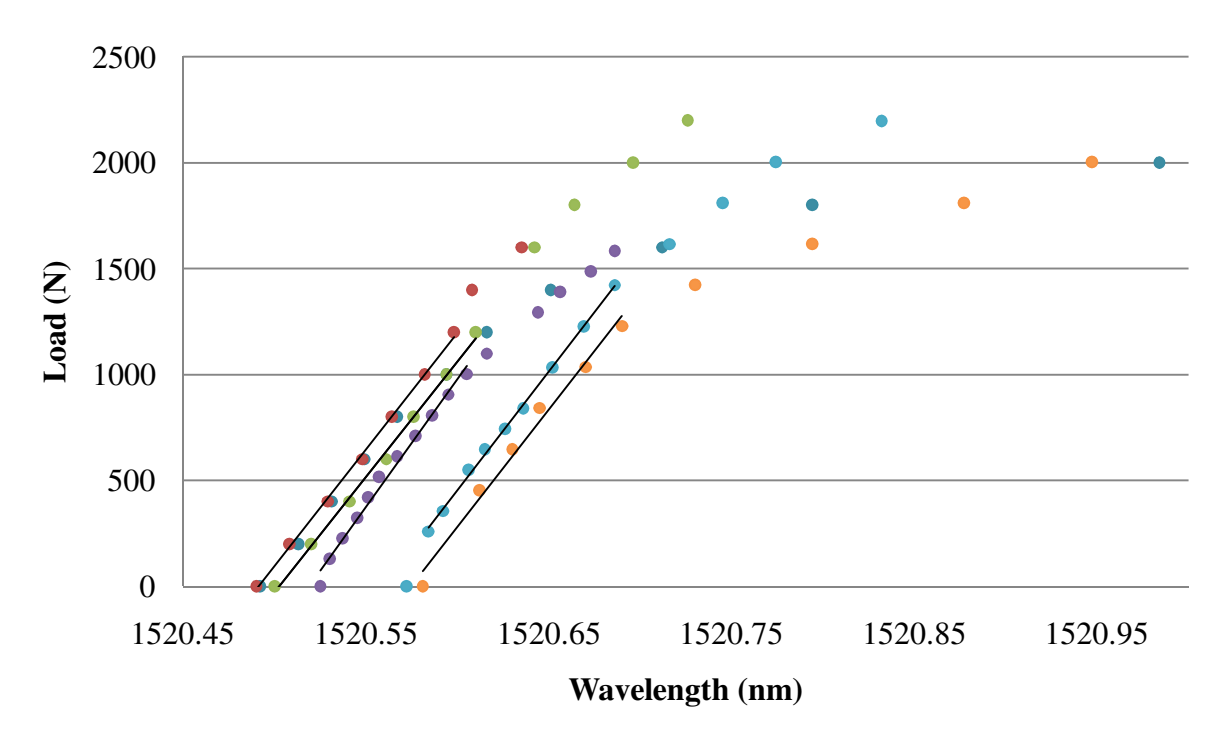


Figure 37: Calibration of the novel preload sensor.

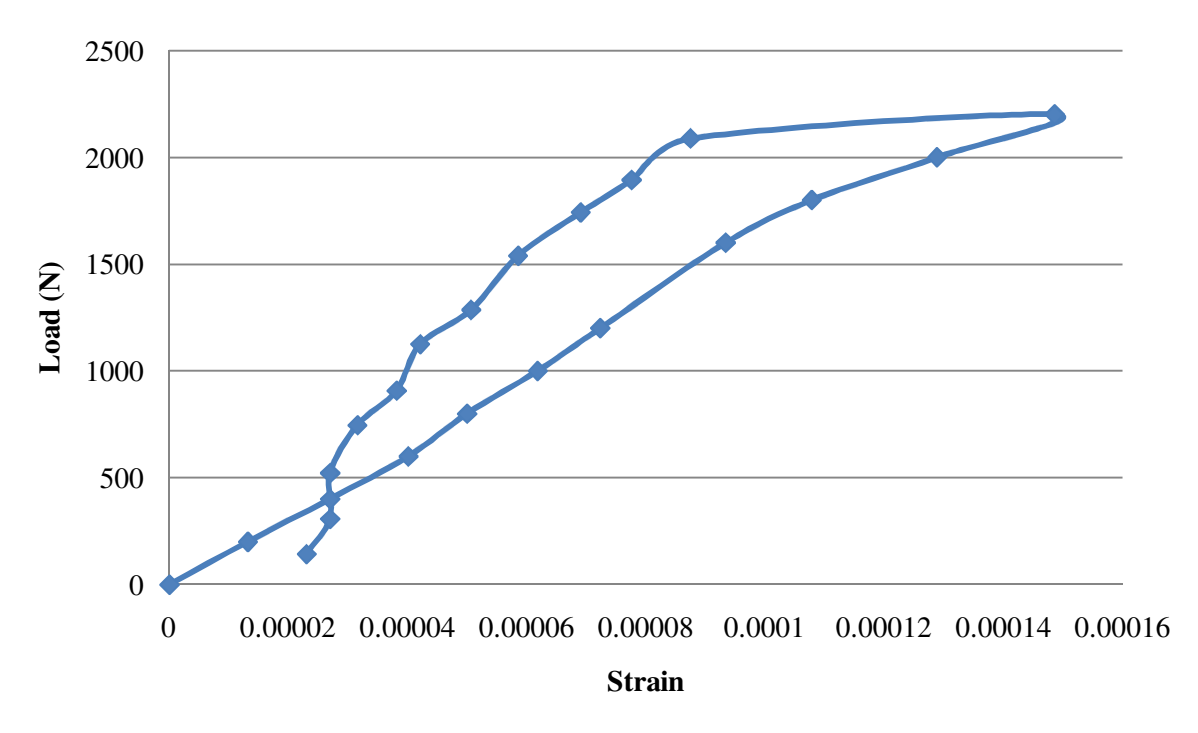


Figure 38: Strain vs. load for loading and unloading of the novel preload sensor.

Preload Testing Parameters

For testing the effects of preload, the samples are all produced to the same dimensions as the baseline tests. This will allow the tests to be conducted with minimal interference from outside factors. The uniformity between tests also gives the opportunity to compare the tests. The only parameters being changed between these tests and the base line are that the preload will be specified at different values instead of the torque. Unfortunately the preload sensor is not reliable enough for the testing. So the load cell will be placed in the joint to ensure the proper preload is applied.

The preloads to be tested are chosen based on the bolt yield characterization performed during the creation of the novel preload sensor. The preloads for the tests will be 500, 2000, and 3500 N. The 500 N preload corresponds to a low amount of preload where the yield characterization was yet to be linear as in Figure 35. 2000 N is in the middle of the values in the linear range of the bolt. 3500 N is still in the linear range but close to the yield allowing for a high amount of preload.

Preload Testing Results

The results for the preload testing are displayed in Figure 38. Notice the tight packing of the 500 N and 2 kN preloaded samples. During testing the load on the fastener is observed through the load cell. The load during testing is increased past the yield of the bolt for each test. The lower preloads have similar stiffnesses but the overall displacement of the cross head is grouped based on preload. The tests run with 3.5 kN of preload also had closely grouped stiffnesses. The stiffness seen for the 3.5 kN preload is also noticeably higher then the values for the other preloads. The preloads also are seen to limit the kinking of the load displacement graph until higher loads. The ultimate loads of all of the tests are approximately the same averaging approximately 72 kN.

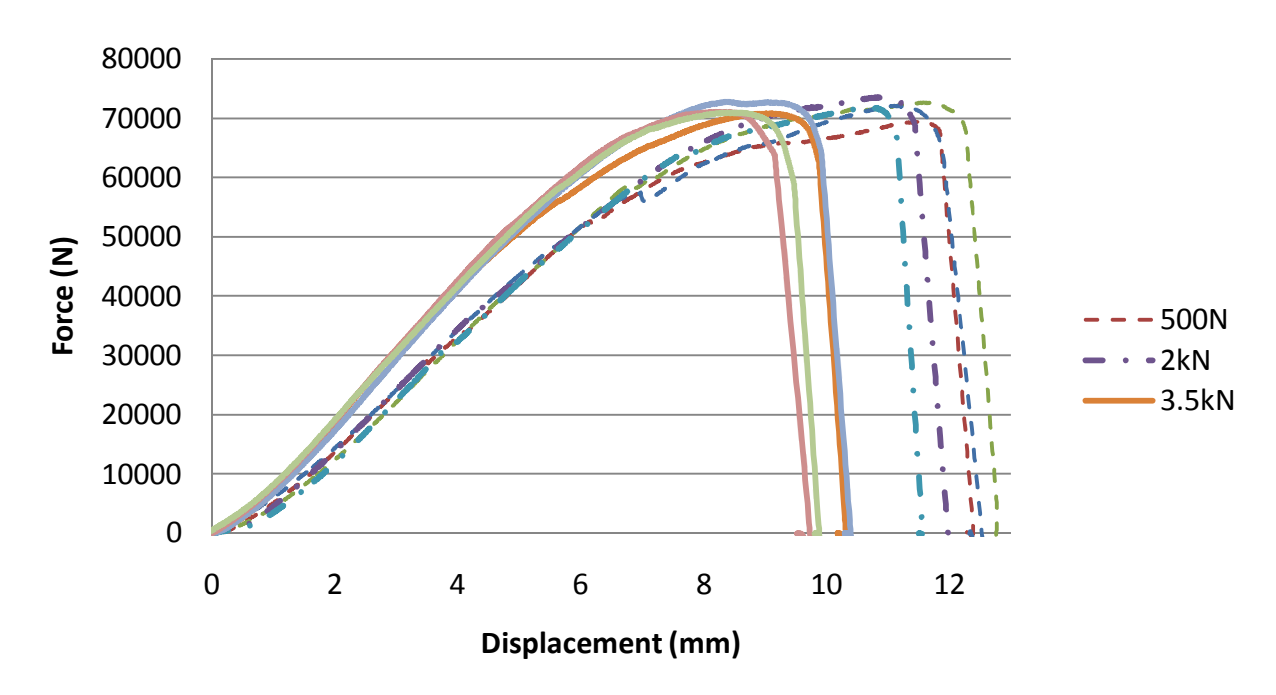


Figure 39: Load vs. displacement results for preload tests.

Table 4: Key values from preload testing.

% Yield	Stiffness (kN/mm)	Initial Failure Load (kN)	Failure Load (kN)	Bearing Stress (MPa)
12	10.4	33.4	71.0	440
61	10.6	34.3	72.6	450
85	12.0	42.8	71.4	443

CHAPTER 5 CONCLUSIONS

This research has provided a new view of how different parameters effect thick composite joints. Thick composite joints are seen to fail in net tension. This was expected from Hou (2003) and caused by the thickness constraint. The trends from these initial tests were seen to continue for the rest of the tests performed through this study. The multiple layer tests show clearly that for the materials tested the single layer panel performs better in stiffness and ultimate failure loads. The increases are seen to be achieved because of the complex loading condition creating higher shear forces on the bonded surface between the multiple layers.

The use of inserts has improved the stiffness by 17.7% - 40.6% for the isotropic aluminum and steel inserts. A great improvement to stiffness was also seen by using the novel insert. The tested configuration was not able to be tested to ultimate failure of the composite, but show promise and could be used with different injectable material. While gains are made in stiffness, no observable difference to either the initial or ultimate failure load was seen. This is assumed to be caused by the thickness constraint forcing the net tension failure.

The FOSG preload sensor was successfully created and for a small number of loadings in the range of 0 to 1200 N. The major problem with the sensor is that strain is stored in the adhesive. The adhesive is assumed to fail slightly with each loading. For this reason, a high strength epoxy is proposed to improve the sensor.

Increasing the preload to 3.5 kN, increased the stiffness of the joint by 15.4% over the 500 N preload. This is considered to happen because of the increased constraint through the thickness. On top of increasing the stiffness, the ultimate failure load increased by 28%. The lower value preloads tested were statistically the same, and we can assume that this is caused by

the increase of load in the fastener during testing. This increase in load pushes the value of load toward yield and thus during the test creates similar conditions.

APPENDIX

APPENDIX

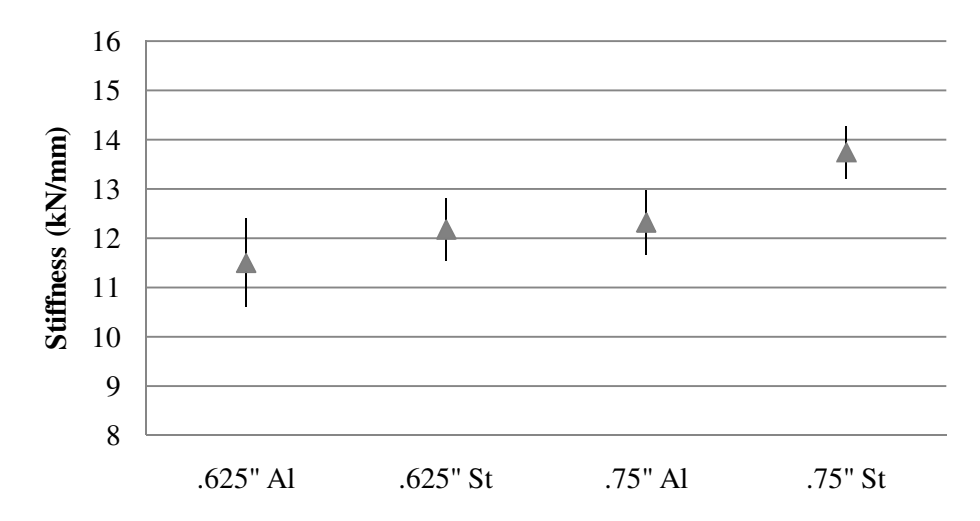


Figure 40: Stiffness values for inserts plotted with error bars.

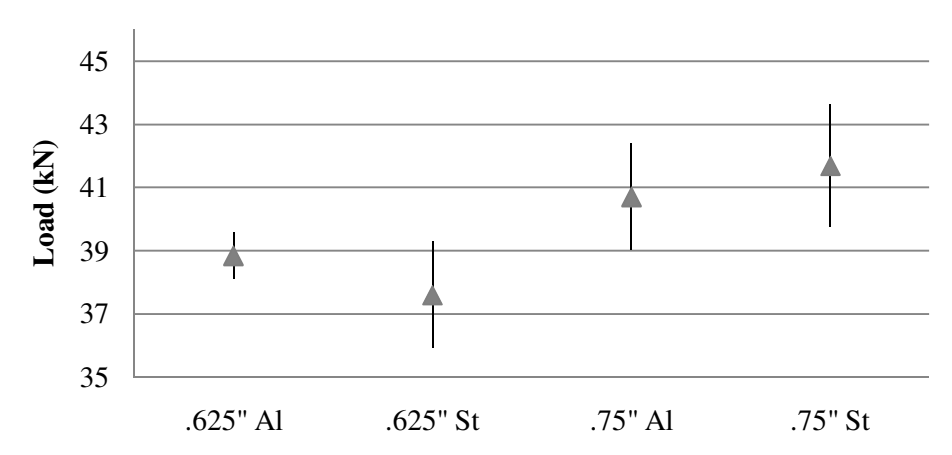


Figure 41: Initial failure values for inserts plotted with error bars.

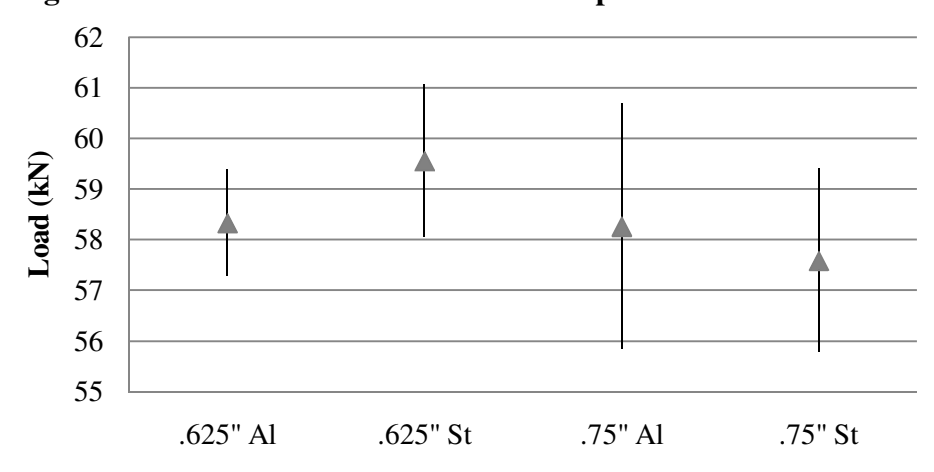


Figure 42: Ultimate failure values for inserts plotted with error bars.

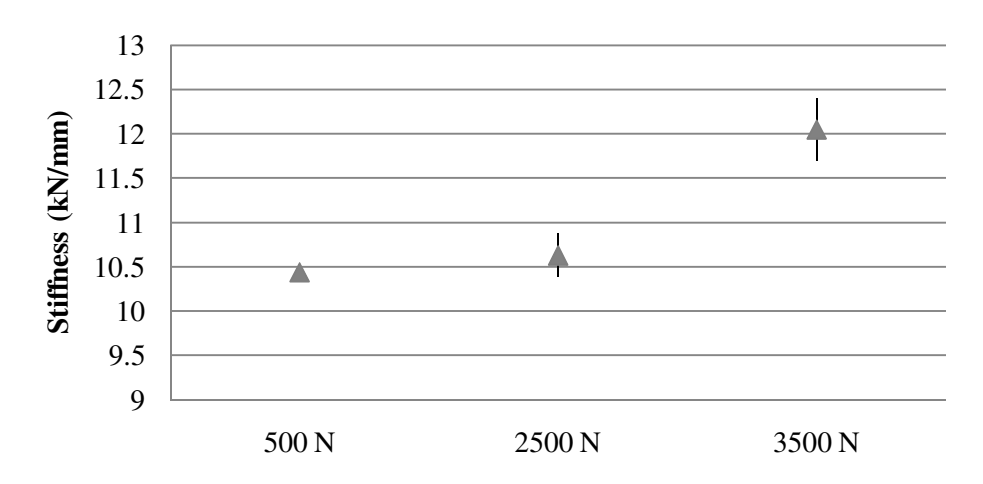


Figure 43: Stiffness values for preloads plotted with error bars.

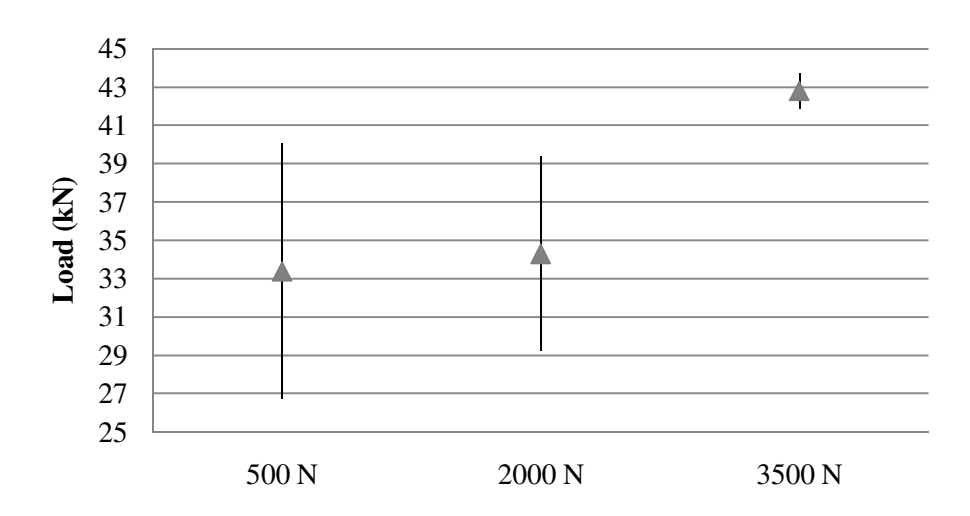


Figure 44: Initial failure values for preloads plotted with error bars.

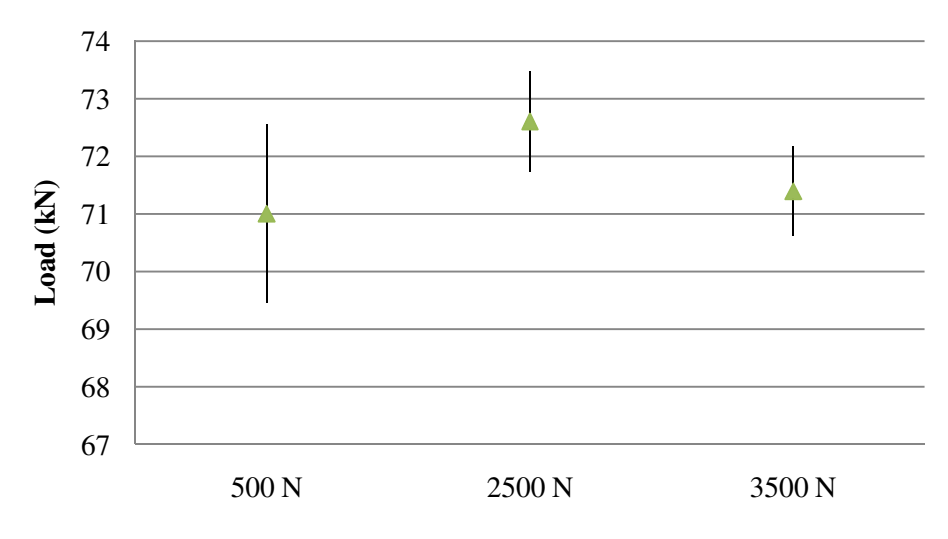


Figure 45: Ultimate failure values for preloads plotted with error bars.

BIBLIOGRAHPY

BIBLIOGRAPHY

Banea, M. D., and. Da Silva, L F M. (2009). Adhesively Bonded Joints in Composite Materials: an Overview. <u>Proceedings of the Institution of Mechanical Engineers</u>, <u>Part L: Journal of Materials: Design and Applications:</u> 223.1, 1-18.

Basu, S. Waas, A.and Ambur, D. (2007). Prediction of Progressive Failure in Multidirectional Composite Laminated Panels. <u>International Journal of Solids and Structures:</u> 44.9, 2648-676.

Bickford, John H. (1995). <u>An Introduction to the Design and Behavior of Bolted Joints</u>. New York: Marcel Dekker.

Budynas, Richard, and J. Keith Nisbett. (2006). <u>Shigley's Mechanical Engineering Design</u> (<u>McGraw-Hill Series in Mechanical Engineering</u>). New York: McGraw-Hill.

Camanho, P., and F. Matthews. (1997). Stress Analysis and Strength Prediction of Mechanically Fastened Joints in FRP: a Review. <u>Composites Part A: Applied Science and Manufacturing</u>: 28.6, 529-47.

Camanho, P.P., Tavares, C.M.L., et al. (2005). Increasing the efficiency of composite single-shear lap joints using bonded inserts. <u>Composites Part B: Engineering</u>: 36, 372-383.

Choi, Jin-Ho, and Young-Jun Chun. (2003). Failure Load Prediction of Mechanically Fastened Composite Joints. <u>Journal of Composite Materials</u>: 37.24, 2163-177.

Cooper, C., and G. J. Turvey. (1995). Effects of Joint Geometry and Bolt Torque on the Structural Performance of Single Bolt Tension Joints in Pultruded GRP Sheet Material. Composite Structures: 32.1-4, 217-26.

Gurvich, M. (1995). Strength Size Effect of Laminated Composites. <u>Composites Science and Technology</u>: 55.1, 93-105.

Herrera-Franco, Pedro J., Cloud, Gary L. (1992). Strain-Relief Inserts for Composite Fasteners – An Experimental Study. <u>Journal of Composite Materials</u>: 26, 751-768.

Heyman, Joseph. (1977). A CW Ultrasonic Bolt-strain Monitor. Experimental Mechanics: 17.5, 183-87.

Hou, L., and D. Liu. (2002). Three-dimensional size effects in composite pin joints." <u>EXPERIMENTAL MECHANICS</u>: 43.2, 115-23.

Hou, L., and D. Liu. (2003). Size effects and thickness constraints in composite joints. JOURNAL OF COMPOSITE MATERIALS: 37.21, 1921-938.

Huang, Y.H. Liu, L. Yeung, T.W. Hung, Y.Y. (2009), Real-time monitoring of clamping force of a bolted joint by use of automatic digital image correlation. <u>Optics & Laser Technology</u>: Volume 41, Issue 4, 408-414.

Jhang KY, Quan HH, Ha J, and Kim NY. (2006). Estimation of Clamping Force in High-tension Bolts through Ultrasonic Velocity Measurement. <u>Ultrasonics</u>: 1339-342.

Khashaba, U., H. Sallam, A. Alshorbagy, and M. Seif. (2006). Effect of Washer Size and Tightening Torque on the Performance of Bolted Joints in Composite Structures. <u>Composite</u> Structures: 73.3, 310-17.

Kim, N. -S. and N. -S. Cho. (2004). Estimating Deflection of a Simple Beam Model Using Fiber Optic Bragg-grating Sensors. <u>Experimental Mechanics</u>: 44.4, 433-39.

Matou, K. (2004). Analysis of Tongue and Groove Joints for Thick Laminates. <u>Composites Part B: Engineering</u>: 35.6-8, 609-17.

Nassar, Sayed, and Meng Aidong. (2007). Optical Monitoring of Bolt Tightening Using 3D Electronic Speckle Pattern Interferometry. Journal of Pressure Vessel Technology: 129.1, 89-95.

Nillsson, Sören. (1989). Increasing Strength of Graphite/Epoxy Bolted Joints by Introducing an Adhesively Bonded Metallic Insert. <u>Journal of Composite Materials</u>: 23, 642-650

Pakdil, M., F. Sen, O. Sayman, and S. Benli. (2007). The Effect of Preload on Failure Response of Glass-Epoxy Laminated Composite Bolted-Joints with Clearance. <u>Journal of Reinforced Plastics and Composites</u>: 26.12, 1239-252.

Pekbey, Y. (2008). The bearing strength and failure behavior of bolted E-glass/epoxy composite joints. Mechanics of Composite Materials: 44.4, 397-414.

Sayman, Onur, Ramazan Siyahkoc, Faruk Sen, and Resat Ozcan. (2007). Experimental determination of bearing strength in fiber reinforced laminated composite bolted joints under preload. <u>Journal of Reinforced Plastics and Composites</u>: 26.10, 1051-063.

Serge M. Melle, Kexing Liu, and Raymond M. Measures. (1993). Practical fiber-optic Bragg grating strain gauge system. <u>Applied Optics</u>: 32, 3601-3609.

Shantha, K.L., S. Thennarasu, and N. Krishnamurti. (1989). Developments and Applications of Cyanoacrylate Adhesives. <u>Journal of Adhesion Science and Technology</u>: 3.1, 237-60.

Thoppul, Srinivasa D., Joana Finegan, and Ronald F. Gibson. (2009). Mechanics of Mechanically Fastened Joints in Polymer matrix Composite Structures: A Review. <u>Composites Science and Technology</u>: 69.3-4, 301-29.

Wisnom, M. R. (1999). Size Effects in the Testing in Fibre-composite Materials. <u>Composites Science and Technology:</u> 59.13, 1937-957.